lipid analogs into lipid rafts reconstituted in supported model membrane monolayers. *Proc. Natl Acad. Sci. USA 98*, 10642–10647.

Dietrich, C., B. Yang, T. Fujiwara, A. Kusumi, K. Jacobson. 2002. Relationship of lipid rafts to transient confinement zones detected by single particle tracking. *Biophys. J. 82*, 274–284.

Dykstra, M., A. Cherukuri, H.W. Sohn, S.J. Tzeng, S.K. Pierce. 2003. Location is everything: lipid rafts and immune cell signaling. *Annu. Rev. Immunol. 21*, 457–481.

East, J.M., D. Melville, A.G. Lee. 1985. Exchange rates and numbers of annular lipids for the calcium and magnesium ion dependent adenosine triphosphatase. *Biochemistry 24*, 2615–2623.

Feder, T.J., I. Brust-Mascher, J.P. Slattery, B. Baird, W.W. Webb. 1996. Constrained diffusion or immobile fraction on cell surfaces: a new interpretation. *Biophys. J. 70*, 2767–2773.

Field, K.A., D. Holowka, B. Baird. 1995. Fc epsilon RI-mediated recruitment of p53/56^{lyn} to detergent-resistant membrane domains accompanies cellular signaling. *Proc. Natl Acad. Sci. USA 92*, 9201–9205.

Field, K.A., D. Holowka, B. Baird. 1997. Compartmentalized activation of the high affinity immunoglobulin E receptor within membrane domains. *J. Biol. Chem. 272*, 4276–4280.

Fra, A.M., E. Williamson, K. Simons, R.G. Parton. 1994. Detergent-insoluble glycolipid microdomains in lymphocytes in the absence of caveolae. *J. Biol. Chem. 269*, 30745–30748.

Gaidarov, I., F. Santini, R.A. Warren, J.H. Keen. 1999. Spatial control of coated-pit dynamics in living cells. *Nat. Cell Biol. 1*, 1–7.

Gil, T., J.H. Ipsen, O.G. Mouritsen, M.C. Sabra, M.M. Sperotto, M.J. Zuckermann. 1998. Theoretical analysis of protein organization in lipid membranes. *Biochim. Biophys. Acta 1376*, 245–266.

Glebov, O.O., B.J. Nichols. 2004. Lipid raft proteins have a random distribution during localized activation of the T-cell receptor. *Nat. Cell Biol. 6*, 238–243.

Hancock, J.F. 2003. Ras proteins: different signals from different locations. *Nat. Rev. Mol. Cell Biol. 4*, 373–384.

Harder, T., P. Scheiffele, P. Verkade, K. Simons. 1998. Lipid domain structure of the plasma membrane revealed by patching of membrane components. *J. Cell Biol. 141*, 929–942.

Heerklotz, H. 2002. Triton promotes domain formation in lipid raft mixtures. *Biophys. J. 83*, 2693–2701.

Heerklotz, H., H. Szadkowska, T. Anderson, J. Seelig. 2003. The sensitivity of lipid domains to small perturbations demonstrated by the effect of Triton. *J. Mol. Biol. 329*, 793–799.

Horvath, L.I., P.J. Brophy, D. Marsh. 1988. Exchange rates at the lipid–protein interface of myelin proteolipid protein studied by spin-label electron spin resonance. *Biochemistry 27*, 46–52.

Iino, R., I. Koyama, A. Kusumi. 2001. Single molecule imaging of green fluorescent proteins in living cells: E-cadherin forms oligomers on the free cell surface. *Biophys. J. 80*, 2667–2677.

Janes, P.W., S.C. Ley, A.I. Magee. 1999. Aggregation of lipid rafts accompanies signaling via the T cell antigen receptor. *J. Cell Biol. 147*, 447–461.

Jordan, B.A., L.A. Devi. 1999. G-protein-coupled receptor heterodimerization modulates receptor function. *Nature 399*, 697–700.

Kawasaki, K., J.J. Yin, W. K. Subczynski, J. S. Hyde, A. Kusumi. 2001. Pulse EPR detection of lipid exchange between protein-rich raft and bulk domains in the membrane: methodology development and its application to studies of influenza viral membrane. *Biophys. J. 80*, 738–748.

Kenworthy, A.K., M. Edidin. 1998. Distribution of a glycosylphosphatidylinositol-anchored protein at the apical surface of MDCK cells examined at a resolution of <100 Å using imaging fluorescence resonance energy transfer. *J. Cell Biol. 142*, 69–84.

Kenworthy, A. K., N. Petranova, M. Edidin. 2000. High-resolution FRET microscopy of cholera toxin B-subunit and GPI-anchored proteins in cell plasma membranes. *Mol. Biol. Cell 11*, 1645–1655.

Kenworthy, A.K., B.J. Nichols, C.L. Remmert G.M. Hendrix, M. Kumar, J. Zimmerberg, J. Lippincott-Schwartz. 2004. Dynamics of putative raft-associated proteins at the cell surface. *J. Cell Biol. 165*, 735–746.

Koyama-Honda, I., K. Ritchie, T. Fujiwara, R. Iino, H. Murakoshi, R.S. Kasai, A. Kusumi. 2005. Fluorescence imaging for monitoring the colocalization of two single molecules in living cells. *Biophys. J. 88*, 2126–2136.

Kusumi, A., J.S. Hyde. 1982. Spin-label saturation-transfer electron spin resonance detection of transient association of rhodopsin in reconstituted membranes. *Biochemistry 21*, 5978–5983.

Kusumi, A., I. Koyama-Honda, K. Suzuki. 2004. Molecular dynamics and interactions for creation of stimulation-induced stabilized rafts from small unstable steady-state rafts. *Traffic 5*, 213–230.

Lai, E.C. 2003. Lipid rafts make for slippery platforms. *J. Cell Biol. 162*, 365–370.

Le Du, M.H., T. Stigbrand, M.J. Taussig, A. Menez, E.A. Stura. 2001. Crystal structure of alkaline phosphatase from human placenta at 18 Å resolution. Implication for a substrate specificity. *J. Biol. Chem. 276*, 9158–9165.

Lehto, M.T., F.J. Sharom. 2002. Proximity of the protein moiety of a GPI-anchored protein to the membrane surface: a FRET study. *Biochemistry 41*, 8368–8376.

London, E., D.A. Brown. 2000. Insolubility of lipids in Triton X-100: physical origin and relationship to sphingolipid/cholesterol membrane domains (rafts). *Biochim. Biophys. Acta 1508*, 182–195.

Lukacik, P., P. Roversi, J. White, D. Esser, G.P. Smith, J. Billington, P.A. Williams, P.M. Rudd, M.R. Wormald, D.J. Harvey, M.D. Crispin, C.M. Radcliffe, R.A. Dwek, D.J. Evans, B.P. Morgan, R.A. Smith, S.M. Lea. 2004. Complement regulation at the molecular level: the structure of decay-accelerating factor. *Proc. Natl Acad. Sci. USA 101*, 1279–1284.

Manes, S., R. Ana Lacalle, C. Gomez-Mouton, A.C. Martinez. 2003. From rafts to crafts: membrane asymmetry in moving cells. *Trends. Immunol. 24*, 320–326.

Marwali, M.R., J. Rey-Ladino, L. Dreolini, D. Shaw, F. Takei. 2003. Membrane cholesterol regulates LFA-1 function and lipid raft heterogeneity. *Blood 102*, 215–222.

Maxfield, F.R. 2002. Plasma membrane microdomains. *Curr. Opin. Cell Biol. 14*, 483–487.

Mayor, S., M. Rao. 2004. Rafts: scale-dependent, active lipid organization at the cell surface. *Traffic 5*, 231–240.

Mayor, S., K.G. Rothberg, F.R. Maxfield. 1994. Sequestration of GPI-anchored proteins in caveolae triggered by cross-linking. *Science 264*, 1948–1951.

McConnell, H.M., A. Radhakrishnan. 2003. Condensed complexes of cholesterol and phospholipids. *Biochim. Biophys. Acta 1610*, 159–173.

McConnell, H.M., M. Vrljic. 2003. Liquid–liquid immiscibility in membranes. *Annu. Rev. Biophys. Biomol. Struct. 32*, 469–492.

Mitchell, J.S., O. Kanca, B.W. McIntyre. 2002. Lipid microdomain clustering induces a redistribution of antigen recognition and adhesion molecules on human T lymphocytes. *J. Immunol. 168*, 2737–2744.

Mukherjee, S., F.R. Maxfield. 2004. Membrane domains. *Annu. Rev. Cell Dev. Biol. 20*, 839–866.

Nagle, J.F. 1992. Long tail kinetics in biophysics? *Biophys. J. 63*, 366–370.

Nichols, B.J. 2003. GM_1-containing lipid rafts are depleted within clathrin-coated pits. *Curr. Biol. 13*, 686–690.

Okonogi, T.M., A. Radhakrishnan, H.M. McConnell. 2002. Two fatty acids can replace one phospholipid in condensed complexes with cholesterol. *Biochim. Biophys. Acta 1564*, 1–4.

Paladino, S., D. Sarnataro, R. Pillich, S. Tivodar, L. Nitsch, C. Zurzolo. 2004. Protein oligomerization modulates raft partitioning and apical sorting of GPI-anchored proteins. *J. Cell Biol. 167*, 699–709.

Parmryd, I., J. Adler, R. Patel, A.I. Magee. 2003. Imaging metabolism of phosphatidylinositol 4,5-bisphosphate in T-cell GM_1-enriched domains containing Ras proteins. *Exp. Cell Res. 285*, 27–38.

Parton, R.G., J.F. Hancock. 2001. Caveolin and Ras function. *Methods Enzymol. 333*, 172–183.

Parton, R. G., J. F. Hancock. 2004. Lipid rafts and plasma membrane microorganization: insights from Ras. *Trends Cell Biol. 14,* 141–147.

Pasdar, M., W. J. Nelson. 1988a. Kinetics of desmosome assembly in Madin-Darby canine kidney epithelial cells: temporal and spatial regulation of desmoplakin organization and stabilization upon cell–cell contact. I. Biochemical analysis. *J. Cell Biol. 106,* 677–685.

Pasdar, M., W. J. Nelson. 1988b. Kinetics of desmosome assembly in Madin-Darby canine kidney epithelial cells: temporal and spatial regulation of desmoplakin organization and stabilization upon cell–cell contact. II. Morphological analysis. *J. Cell Biol. 106,* 687–695.

Pasdar, M., W. J. Nelson. 1989. Regulation of desmosome assembly in epithelial cells: kinetics of synthesis, transport, and stabilization of desmoglein I, a major protein of the membrane core domain. *J. Cell Biol. 109,* 163–177.

Pasenkiewicz-Gierula, M., W. K. Subczynski, A. Kusumi. 1991. Influence of phospholipid unsaturation on the cholesterol distribution in membranes. *Biochimie 73,* 1311–1316.

Peters, R., R. J. Cherry. 1982. Lateral and rotational diffusion of bacteriorhodopsin in lipid bilayers: experimental test of the Saffman-Delbruck equations. *Proc. Natl Acad. Sci. USA 79,* 4317–4321.

Pierce, S. K. 2002. Lipid rafts and B-cell activation. *Nat. Rev. Immunol. 2,* 96–105.

Pierini, L. M., F. R. Maxfield. 2001. Flotillas of lipid rafts fore and aft. *Proc. Natl Acad. Sci. USA 98,* 9471–9473.

Pierini, L. M., R. J. Eddy, M. Fuortes, S. Seveau, C. Casulo, F. R. Maxfield. 2003. Membrane lipid organization is critical for human neutrophil polarization. *J. Biol. Chem. 278,* 10831–10841.

Pralle, A., P. Keller, E. L. Florin, K. Simons, J. K. Horber. 2000. Sphingolipid–cholesterol rafts diffuse as small entities in the plasma membrane of mammalian cells. *J. Cell Biol. 148,* 997–1008.

Pribluda, V. S., C. Pribluda, H. Metzger. 1994. Transphosphorylation as the mechanism by which the high-affinity receptor for IgE is phosphorylated upon aggregation. *Proc. Natl Acad. Sci. USA 91,* 11246–11250.

Prior, I. A., C. Muncke, R. G. Parton, J. F. Hancock. 2003. Direct visualization of Ras proteins in spatially distinct cell surface microdomains. *J. Cell Biol. 160,* 165–170.

Radhakrishnan, A., T. G. Anderson, H. M. McConnell. 2000. Condensed complexes, rafts, and the chemical activity of cholesterol in membranes. *Proc. Natl Acad. Sci. USA 97,* 12422–12427.

Radhakrishnan, A., X. M. Li, R. E. Brown, H. M. McConnell. 2001. Stoichiometry of cholesterol–sphingomyelin condensed complexes in monolayers. *Biochim. Biophys. Acta 1511,* 1–6.

Rudd, P. M., B. P. Morgan, M. R. Wormald, D. J. Harvey, C. W. van den Berg, S. J. Davis, M. A. Ferguson, R. A. Dwek. 1997. The glycosylation of the complement regulatory protein, human erythrocyte CD59. *J. Biol. Chem. 272,* 7229–7244.

Saffman, P. G., M. Delbrück. 1975. Brownian motion in biological membranes. *Proc. Natl Acad. Sci. USA 72,* 3111–3113.

Schroeder, R. J., S. N. Ahmed, Y. Zhu, E. London, D. A. Brown. 1998. Cholesterol and sphingolipid enhance the Triton X-100 insolubility of glycosylphosphatidylinositol-anchored proteins by promoting the formation of detergent-insoluble ordered membrane domains. *J. Biol. Chem. 273,* 1150–1157.

Sharma, P., R. Varma, R. C. Sarasij, Ira, K. Gousset, G. Krishnamoorthy, M. Rao, S. Mayor. 2004. Nanoscale organization of multiple GPI-anchored proteins in living cell membranes. *Cell 116,* 577–589.

Sheets, E. D., G. M. Lee, R. Simson, K. Jacobson. 1997. Transient confinement of a glycosylphosphatidylinositol-anchored protein in the plasma membrane. *Biochemistry 36,* 12449–12458.

Sheets, E. D., D. Holowka, B. Baird. 1999. Critical role for cholesterol in Lyn-mediated tyrosine phosphorylation of FcepsilonRI and their association with detergent-resistant membranes. *J. Cell Biol. 145,* 877–887.

Shvartsman, D. E., M. Kotler, R. D. Tall, M. G. Roth, Y. I. Henis. 2003. Differently

anchored influenza hemagglutinin mutants display distinct interaction dynamics with mutual rafts. *J. Cell Biol. 163*, 879–888.

Simons, K., E. Ikonen. 1997. Functional rafts in cell membranes. *Nature 387*, 569–572.

Simons, K., D. Toomre. 2000. Lipid rafts and signal transduction. *Nat. Rev. Mol. Cell Biol. 1*, 31–39.

Simons, K., G. van Meer. 1988. Lipid sorting in epithelial cells. *Biochemistry 27*, 6197–6202.

Simons, K., W. L. Vaz. 2004. Model systems, lipid rafts, and cell membranes. *Annu. Rev. Biophys. Biomol. Struct 33*, 269–295.

Singer, S.J., G.L. Nicolson. 1972. The fluid mosaic model of the structure of cell membranes. *Science 175*, 720–731.

Stoddart, A., M.L. Dykstra, B.K. Brown, W. Song, S.K. Pierce, F.M. Brodsky. 2002. Lipid rafts unite signaling cascades with clathrin to regulate BCR internalization. *Immunity 17*, 451–462.

Subczynski, W.K., A. Kusumi. 2003. Dynamics of raft molecules in the cell and artificial membranes: approaches by pulse EPR spin labeling and single molecule optical microscopy. *Biochim. Biophys. Acta 1610*, 231–243.

Subczynski, W.K., W.E. Antholine, J.S. Hyde, A. Kusumi. 1990. Microimmiscibility and three-dimensional dynamic structures of phosphatidylcholine–cholesterol membranes: translational diffusion of a copper complex in the membrane. *Biochemistry 29*, 7936–7945.

Suzuki, K., F. Sanematsu, T. Fujiwara, M. Edidin, A. Kusumi. 2001. Rapid, continual formation/dispersion of raft-like domains in the resting cell membrane. *Mol. Biol. Cell 12*, 470a.

Suzuki, K., F. Sanematsu, T. Fujiwara, M. Edidin, A. Kusumi. 2002. Stimulation-induced formation of temporal but stabilized rafts. *Biophys. J. 82*, 348a.

Suzuki, K., F. Sanematsu, T. Fujiwara, K. Ritchie, M. Edidin, A. Kusumi. 2003. Crosslinking of a GPI-anchored protein creates signaling rafts from smaller, transient, lipid rafts. *Biophys. J. 84*, 487a.

Tavano, R., G. Gri, B. Molon, B. Marinari, C.E. Rudd, L. Tuosto, A. Viola. 2004. CD28 and lipid rafts coordinate recruitment of Lck to the immunological synapse of human T lymphocytes. *J. Immunol. 173*, 5392–5397.

Thomas, J.L., D. Holowka, B. Baird, W.W. Webb. 1994. Large-scale co-aggregation of fluorescent lipid probes with cell surface proteins. *J. Cell Biol. 125*, 795–802.

Varma, R., S. Mayor. 1998. GPI-anchored proteins are organized in submicron domains at the cell surface. *Nature 394*, 798–801.

Vaz, W.L., M. Criado, V.M. Madeira, G. Schoellmann, T.M. Jovin. 1982. Size dependence of the translational diffusion of large integral membrane proteins in liquid-crystalline phase lipid bilayers. A study using fluorescence recovery after photobleaching. *Biochemistry 21*, 5608–5612.

Vrljic, M., S.Y. Nishimura, S. Brasselet, W.E. Moerner, H.M. McConnell. 2002. Translational diffusion of individual class II MHC membrane proteins in cells. *Biophys. J. 83*, 2681–2692.

Wu, M., D. Holowka, H.G. Craighead, B. Baird. 2004. Visualization of plasma membrane compartmentalization with patterned lipid bilayers. *Proc. Natl Acad. Sci. USA 101*, 13798–13803.

Young, R.M., D. Holowka, B. Baird. 2003. A lipid raft environment enhances Lyn kinase activity by protecting the active site tyrosine from dephosphorylation. *J. Biol. Chem. 278*, 20746–20752.

European Journal of Neuroscience, Vol. 25, pp. 406–416, 2007 doi:10.1111/j.1460-9568.2007.05282.x

Truncated TrkB-T1 regulates the morphology of neocortical layer I astrocytes in adult rat brain slices

Koji Ohira,[1,2,3] Nobuo Funatsu,[1] Koichi J. Homma,[4] Yoshinori Sahara,[1] Motoharu Hayashi,[5] Takeshi Kaneko,[2,3] and Shun Nakamura[1,3]

[1]Department of Biochemistry and Cellular Biology, National Institute of Neuroscience, National Center of Neurology and Psychiatry, 4-1-1 Ogawahigashi, Kodaira, Tokyo 187–8502, Japan
[2]Department of Morphological Brain Science, Graduate School of Medicine, Kyoto University, Kyoto 606–8501, Japan
[3]Core Research for Evolutional Science and Technology (CREST), Japan Science and Technology Agency, Saitama 332–0012, Japan
[4]Department of Molecular Pathology, Faculty of Pharmaceutical Sciences, Teikyo University, Kanagawa 199–0195, Japan
[5]Department of Cellular and Molecular Biology, Primate Research Institute, Kyoto University, Aichi 484–8506, Japan

Keywords: BDNF, electroporation, neurotrophin, RNA interference

Abstract

By altering their morphology, astrocytes, including those involved in the maintenance and plasticity of neurons and in clearance of transmitter, play important roles in synaptic transmission; however, the mechanism that regulates the morphological plasticity of astrocytes remains unclear. Recently, we reported that T1, a subtype of TrkB (a family of BDNF-specific receptors), altered astrocytic morphology through the control of Rho GTPases in primary astrocyte cultures. In this study, we extended this observation to investigate acute neocortical slices from adult rats. T1 siRNA-expression vectors were electroporated into astrocytes in neocortical layer I of living rats. In both normal slices and control vector-electroporated slices, BDNF induced the elongation of the astrocytic processes and increased the branching of processes in slices after 1 h incubation. In contrast, in T1 siRNA-electroporated slices, no such significant morphological changes were observed in the astrocytes. In addition, the number of synaptophysin$^+$ sites in contact with GFAP$^+$ processes increased in a BDNF–T1-dependent manner without the increase in the total synaptophysin$^+$ sites. Therefore, the present study provides evidence of the regulation of layer I astrocytic morphology by the BDNF–T1 signal in adult rat neocortical slices.

Introduction

Neurotrophins and their specific tropomyosin-related kinase (Trk) receptors are known to be involved in the regulation of cell morphology during development (Bibel & Barde, 2000). Neurotrophins (NTs) belong to the nerve growth factor (NGF)-related gene family: NGF, brain-derived neurotrophic factor (BDNF), NT-3, and NT4/5. The Trk receptor family consists of three members: TrkA for NGF, TrkB for BDNF and NT-4/5, and TrkC for NT-3 (Barbacid, 1994). The *trkB* gene encodes at least three receptor subtypes (Klein *et al.*, 1990; Middlemas *et al.*, 1991). One such subtype is the full-length form (TK+) that includes tyrosine kinase in the cytosolic domain. The other two subtypes, T1 and T2, lack tyrosine kinases. T1 is expressed in both neurons and glial cells (Armanini *et al.*, 1995; Ohira *et al.*, 2005a, 2005b) whereas T2 is expressed primarily in neurons (Armanini *et al.*, 1995).

Recent studies have shed light on interactions between neurons and glial cells (Fellin & Carmignoto, 2004). In particular, it has been demonstrated that calcium entry into astrocytes modulates synaptic transmission (Bezzi *et al.*, 2004; Fiacco & McCarthy, 2004). In addition, astrocytic endfeet enwrap synapses (Ventura & Harris, 1999), i.e. those synapses referred to as tripartite synapses (Araque *et al.*, 2001). Interestingly, astrocytic processes surrounding active synapses are able to rapidly alter their morphology in acute slices from the brainstem (Hirrlinger *et al.*, 2004), hypothalamus (Langle *et al.*, 2003) and hippocampus (Benediktsson *et al.*, 2005) of infant- to pubertal-stage rodents. In contrast, alterations of fine neuronal structures such as dendrites and spines in the neocortex of adult mice hardly occur under normal conditions (Grutzendler *et al.*, 2002). Such results have suggested that the morphological alteration of astrocytes might be essential for the maintenance and plasticity of synaptic transmission, as well as for transmitter clearance. Therefore, it would be of great interest to clarify the mechanism(s) responsible for controlling astrocytic morphology.

Recently, we reported that T1 regulates astrocytic morphology via Rho GTPases in primary astrocyte cultures (Ohira *et al.*, 2005a). T1 also controls calcium entry into astrocytes (Rose *et al.*, 2003). In addition, BDNF release is highly regulated by neuronal activity (Hartmann *et al.*, 2001; Kohara *et al.*, 2001). Thus, these findings led us to postulate that BDNF release due to neuronal activity might induce morphological changes in astrocytes in the CNS.

For the initial evaluation of this hypothesis, we investigated the role played by endogenous T1 in the regulation of astrocytic morphology in acute slices of the adult rat neocortex. Using T1 small interfering RNA (siRNA)-expressing vectors that were electroporated into neocortical layer I of adult rats, we demonstrated that T1 regulated astrocytic

Correspondence: Dr Shun Nakamura, [1]Department of Biochemistry and Cellular Biology, as above.
E-mail: nakamura@ncnp.go.jp

Received 13 March 2006, revised 5 November 2006, accepted 7 November 2006

morphology in a BDNF-dependent manner. Therefore, considering that astrocytes modulate synaptic transmission (Bezzi *et al.*, 2004; Fiacco & McCarthy, 2004), these results indicate that the morphological changes regulated by the BDNF–T1 signal in astrocytes might play important roles in adult synaptic plasticity in the neocortex.

Materials and methods

T1 siRNA vector

The T1 siRNA vector was produced using the BLOCK-iT U6 Entry Vector kit (Invitrogen, Carlsbad, CA, USA). The pENTR/U6 vector integrates the human U6 promoter which drives RNA polymerase III. Generally, transcription by RNA polymerase III produces a higher amount of RNA than that by RNA polymerase II. Moreover, the U6 promoter belongs to a type III polymerase promoter, which is suitable for expressing a short-length RNA such as short hairpin RNA and micro RNA, for use in RNA interference because there is no internal promoter in it.

Briefly, 5′ oligo CAGCGTCATAAGATCCCCCTGGATGAGAATCCAGGGGGATCTTATGA and 3′ oligo AAAATCATAAGATCCCCCTGGATTCTCATCCAGGGGGATCTTATGAC were incubated at 95 °C for 4 min. The mixture was cooled to room temperature for 10 min to generate the double-strand oligo. The double-strand oligo was cloned into the pENTR/U6 vector. For the control oligos, 5′ oligo CAGCGAAGATCCCCCTGGATGGGAACGCCCATCCAGGGGGATCTT and 3′ oligo AAAAAAGATCCCCCTGGATGGGCGTTCCCATCCAGGGGGATCTTC were used.

Western blot analysis

C6 cells (Dainippon Pharmaceutical, Osaka, Japan) were maintained in Ham's F-10 medium (Gibco, Rockville, MD, USA) supplemented with 15% horse serum (Gibco) and 2.5% fetal bovine serum (Gibco) in a humidified atmosphere containing 5% CO_2 at 37 °C. The vectors (2 μg per 6-cm dish) were transfected into C6 cells (50% confluent) with FuGENE6 (Roche, Basel, Switzerland; Wiesenhofer *et al.*, 1999). The transfection efficiency of the green fluorescent protein (GFP) expression vector was ~60%. After 24 h, the cells were lysed in lysis buffer (Tris-HCl, pH 7.5, 50 mM; NaCl, 150 mM; $MgCl_2$, 5 mM; Triton X-100, 0.5%; PMSF, 1 mM; leupeptin, 10 μg/mL; and aprotinin, 20 μg/mL). After the lysed cells were centrifuged at 10 000 *g* at 4 °C for 20 min, the supernatants were mixed with 4 × sodium dodecyl sulphate (SDS) sample buffer and boiled for 3 min. Samples (5 μg/lane for actin and tubulin, 100 μg/lane for T1) were subjected to SDS–polyacrylamide gel electrophoresis (7% gel for T1, 12% gel for actin and tubulin), and the proteins were blotted onto polyvinylidene difluoride membranes (Millipore, Billerica, MA, USA). The membranes were blocked in 5% skimmed milk in phosphate-buffered saline (PBS; in mM: NaCl, 137; Na_2HPO_4, 8.1; KCl, 2.7; and KH_2PO_4, 1.5). After incubation of the blots with antibodies (anti-T1, diluted at 1 : 200; Santa Cruz Biotech., Santa Cruz, CA, USA; antiactin, diluted at 1 : 200; and antitubulin, diluted at 1 : 200; both Sigma, St Louis, MO, USA) at room temperature for 1 h, they were incubated with secondary antibodies conjugated with horseradish peroxidase and the proteins were visualized by the enhanced chemiluminescence system (Amersham Pharmacia Biotech, Tokyo, Japan). The specificity of anti-T1 antibody for use with Western blot analysis and immunohistochemistry has already been assessed in our previous studies (Ohira *et al.*, 1999; Ohira & Hayashi, 2003). For the quantitative analysis of protein bands we measured the band areas using ImageJ software.

Electroporation

The methods were approved by the National Institute of Neuroscience Committee for the Ethical use of Experimental Animals, based on the guiding principles of the Council for International Organizations of Medical Sciences (1984). Every effort was made to minimize the number of animals used. Adult male Sprague–Dawley (S-D) rats (4–6 weeks, $n = 10$) were deeply anaesthetized with sodium pentobarbital (50 mg/kg). A rectangular hole in the right hemisphere of the skull (3 mm wide and 5 mm long) was created. After an anode tungsten needle was stereotaxically and diagonally inserted under the neocortex (2 mm posterior and 3.5 mm lateral to the bregma, at an angle of 20° to the brain surface), a mixture of 20 μL (GFP : siRNA, 1 : 5) of GFP plasmid vector solution (pCA-GFP; 1 μg/μL in 0.01% Fast Green in Tyrode's solution) and T1 siRNA (1 μg/μL) or the control vectors (1 μg/μL) was injected between the arachnoid and the dura using a pipette (P-20; Gilson, Middleton, WI, USA) connected to a silicon tube and a 27-gauge injection needle (Terumo, Tokyo, Japan). The rectangular platinum plate cathode (1 mm wide and 1.5 mm long) was placed on the dura, and a series of five square pulses (50 ms, 15 V, 950-ms intervals) were immediately sent using Electro Square Porator model T820 and Optimizor 500 (BTX, Harvard Apparatus, Holliston, MA, USA). At 3 days after electroporation, the rats were killed and the brains were removed in order to prepare acute slices.

Morphological assay

Rats were anaesthetised with pentobarbital sodium (25 mg/kg i.p.). After decapitation, the brains were removed from normal (4–6 weeks S-D rat, $n = 10$) and electroporated rats (4–6 weeks S-D rat, $n = 10$) and yellow fluorescent protein (YFP) transgenic mice [4–6 weeks, $n = 3$; B6.Cg-Tg (Thy1-YFP) 16Jrs/J, The Jackson Laboratory, Bar Harbor, ME, USA], and 500-μm slices were created. The slices were kept for 30 min at 4 °C in DMEM (Invitrogen, Carlsbad, CA, USA) containing N2 supplement (Invitrogen). For the administration of reagents, the slices were stimulated for 60 min at 37 °C and 5% CO_2 with 20 ng/mL BDNF (PeproTech, Rocky Hill, NJ, USA) or 100 ng/mL NGF (PeproTech). The dishes were agitated gently during incubation. Then, the slices were fixed at 4 °C for 1 h in 4% PFA in PBS. For cryoprotection, they were sequentially immersed in 5, 10, 20 and 30% sucrose. Thereafter, the slices were further sliced into 10-μm-thick sections and were incubated with the primary antibodies at 4 °C for 48 h. For the double staining analysis, we used the following primary antibodies: the rabbit polyclonal antibodies were antiglial fibrillary acidic protein (GFAP; diluted at 1 : 50; Sigma) and anti-T1 (diluted at 1 : 1600; Santa Cruz Biotech.); and the mouse monoclonal antibodies were antiglutamic acid decarboxylase 65/67 (diluted at 1 : 10 000; Affinity Research Products, Exeter, UK), anti-GFAP (diluted at 1 : 1000; Chemicon, Temecula, CA, USA), and antisynaptophysin (diluted at 1 : 1000; Chemicon). For the T1 staining procedure, in order to retrieve antigenicity the samples were preincubated in 6 M guanidine chloride in 50 mM Tris-HCl, pH 10.2, for 15 min at room temperature (Ohira *et al.*, 2003, 2004, 2005a, 2005b). For the morphological analyses of the astrocytes, the parameters were defined as follows: a thick process that extended radially from a soma was defined as a primary process, and a fine process that extended from a primary process was designated a branch. For the analysis of synaptophysin-positive ($^+$) sites, the number of sites per 14 500 μm^2 was counted. For the analysis of the interaction among synaptophysin$^+$ sites and GFAP$^+$ processes, the number of synaptophysin$^+$ sites that were piled on (white in Fig. 6A and B) or contacted with GFAP$^+$ processes (blue in Fig. 6A and B) was counted

in an area of 14 500 μm^2. The samples in a 0.5-μm-thick plane were analysed using a confocal microscope (TCS SP2; Leica, Wetzlar, Germany). In this assay, we chose the layer I areas to be analysed at random.

For the quantitative analysis of *in vivo* fluorescent intensity of T1, the images of astrocytes were taken under the same condition. Fluorescent intensity was measured with ImageJ software.

Terminal deoxynucleotidyl transferase-mediated digoxigenin nucleotide nick-end labelling (TUNEL) staining

Apoptotic cells were identified by using modified ApopTag apoptosis detection systems (Serologicals, Norcross, GA, USA). For the analyses of injured cortices, young adult male S-D rats (4–6 weeks, $n = 3$) were deeply anaesthetized with sodium pentobarbital (50 mg/kg). Rectangular holes were bored into the skull (3 mm wide and 5 mm long) over the right hemisphere. The motor cortex was injured by the application of a surgical knife attached to the tip of the vertical bar of the stereotaxic instrument; this procedure was performed according to the stereotaxic brain atlas (Paxinos & Watson, 1986). The stereotaxic coordinates used for cutting were as follows: anteroposterior, +1 to −1.5 mm from bregma; lateral, 4 mm from the midline; and depth, 1 mm below the brain surface. At 2 days after the operation, the brains were fixed in 4% PFA. The brain sections (10 μm) from the injured and electroporated rats were incubated with terminal deoxynucleotidyl transferase for 1 h at 37 °C. Thereafter, the sections were stained with antidigoxigenin (Roche Applied Science, Basel, Switzerland) and with secondary antibody conjugated with Cy3 (Chemicon). Nuclei were stained with Hoechst 33258 (Sigma).

Data collection

In the following two analyses (the astrocytic morphology and the relationship between $GFAP^+$ processes and $synaptophysin^+$ sites), we obtained the data from 10 normal rats, five control vector-electroporated rats and five T1 siRNA vector-electroporated rats. In addition, one control and one siRNA vector-electroporated rat was subjected to each analysis.

In order to analyse astrocytic morphology, we collected data from 57 cells in normal slices not treated with BDNF, 63 cells in normal slices treated with BDNF, 62 cells in normal slices not treated with NGF, 60 cells in normal slices treated with NGF, 71 cells in control vector-electroporated slices not treated with BDNF, 75 cells in control vector-electroporated slices treated with BDNF, 71 cells in siRNA vector-electroporated slices not treated with BDNF and 66 cells in siRNA vector-electroporated slices treated with BDNF. For the analysis of the relationship between $GFAP^+$ processes and $synaptophysin^+$ sites, the data was obtained from the following: 44 normal sections not treated with BDNF, 47 normal sections treated with BDNF, 43 normal sections not treated with NGF, 45 sections treated with NGF, 47 control vector-electroporated sections not treated with BDNF, 46 control vector-electroporated sections treated with BDNF, 49 siRNA vector-electroporated sections not treated with BDNF and 48 siRNA vector-electroporated sections treated with BDNF.

Results

BDNF-dependent morphological change in astrocytes in neocortical layer I of acute slices prepared from adult rats

Astrocytes in the CNS are generally divided into two groups, fibrous and protoplasmic astrocytes. Fibrous astrocytes are characterized by (i) long processes with slight branching, (ii) GFAP-rich contents and (iii) distribution in the white matter and in neocortical layer I. Protoplasmic astrocytes have the following typical features: (i) well-branching short processes, (ii) low GFAP content and (iii) distribution in the grey matter (Peters *et al.*, 1976; Raff *et al.*, 1983; Miller & Raff, 1984). In the present study an immunofluorescent approach was used to observe layer I fibrous astrocytes, but the protoplasmic astrocytes in layers II–VI were not observed. As GFAP was observed in large amounts in the layer I fibrous astrocytes, a double-immunofluorescence study of GFAP and T1 enabled the visualization of layer I fibrous astrocytes (Fig. 1A). Also, the layer I fibrous astrocytes do not overlap their neighbours' space (Fig. 2). Similarly, the protoplasmic astrocytes in hippocampal CA1 stratum radiatum have separate domains (Bushong *et al.*, 2002). Therefore, we were able to observe individual astrocytes without any intermingling. Moreover, in our preliminary study we visualized the morphology of astrocytes in neocortical layer I of acute brain slices prepared from developing mice (postnatal days 14–20) using a combination of intracellular recording, biocytin injection and coimmunofluorescent staining with GFAP. These findings were in contrast to those obtained with protoplasmic astrocytes, in which GFAP only enables the visualization of ~15% of the total cell volume in the hippocampal CA1 (Bushong *et al.*, 2002). The layer I astrocytes exhibited a mean resting membrane potential of −77.3 ± 7.0 mV (total $n = 8$ cells), and did not produce action potentials. The morphology revealed by biocytin injection into glial cells that had been electrophysiologically identified was consistent with that of neocortical layer I astrocytes in adult mammals (Colombo *et al.*, 2000). Although this intracellular staining method could reveal the morphology of astrocytes clearly in the developing cortex by 3 weeks postnatal, it was impracticable to make whole-cell patch-clamp recordings of astrocytes in adult slices of mice and rats. Our aim of this study was to determine whether T1 was involved in the regulation of morphological changes in astrocytes in the adult cortex. In this study, therefore, whole-cell patch-clamp recording was abandoned in favour of investigating the morphological changes in astrocytes in the adult cortex. In our rat preparation, a double-immunofluorescence study of GFAP and T1 expression revealed that the cell shape of neocortical layer I astrocytes was quite similar to that observed in the mouse preparation. The length of layer I astrocytes in our study (mean ± SD, 24.5 ± 9.2 μm; total, 194 processes from 57 astrocytes) was similar to the data reported by Colombo *et al.*, 2000). Thus, we concluded that the cell shape observed in the double-immunofluorescence study with GFAP and T1 probably reflects the actual cell bodies and processes of the astrocytes in layer I. We therefore focused on layer I fibrous astrocytes.

As shown in Fig. 1, we observed rapid morphological changes among layer I astrocytes with BDNF treatment for 1 h. BDNF treatment induced process elongation and branching, but it did not lead to an increase in the number of primary processes from each soma. In contrast, NGF treatment had no effect on astrocytic morphological changes. Together with the finding that the layer I astrocytes express mainly T1 *in vivo* (Ohira *et al.*, 2005a), this finding regarding morphological changes among astrocytes is suggestive of an induction by the T1 signalling cascade in the astrocytes themselves.

Effect of T1 siRNA on astrocytic morphology

Next, in order to examine the contribution of T1 to BDNF-dependent morphological changes in astrocytes, we constructed T1 siRNA-expression vectors. Then, using rat glioma C6 cells that intrinsically express T1, we confirmed the RNA interference effect of this vector (Fig. 3). At 24 h after transfection, the expression level of T1 had not changed in the control vector-transfected cells (Fig. 3B). On the other

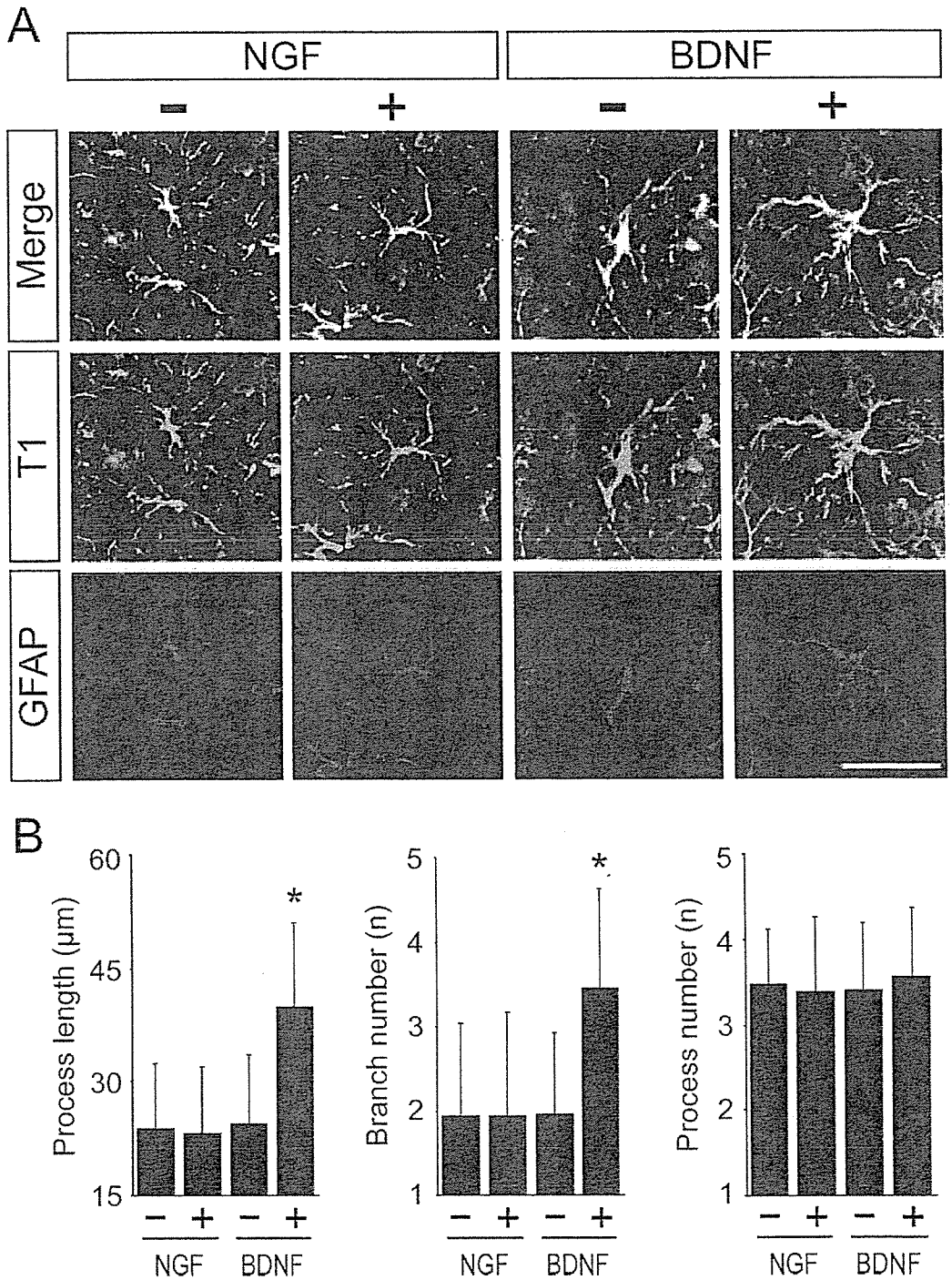

FIG. 1. Morphological changes in astrocytes. (A) Astrocytes in layer I of the motor cortex were stained by anti-T1 (blue) and anti-GFAP (red). (B) Quantitative analyses of process length (left panel), number of branches (middle panel) and number of processes (right panel). Values are given as means ± SD and are the results of four independent experiments. *$P < 0.05$ (one-way ANOVA and Scheffé's *post hoc* test) compared to the astrocytes in slices not treated with BDNF; –, no stimulation; +, stimulation with NGF or BDNF. Scale bar, 30 μm.

hand, in the T1 siRNA-transfected cells, T1 expression was decreased to 1/4 of the control level (Fig. 3B). Thus, we concluded that the T1 siRNA-expression vectors were effective at suppressing the expression of T1 proteins.

In order to deliver the T1 siRNA-expression vectors into the layer I astrocytes, we performed an electroporation of T1 siRNA-expression vectors into the neocortex of living rats. At 3 days after electroporation, the neocortical slices were subjected to a series of morphological analyses. The vectors were focally electroporated into layer I cells, such that we did not observe GFP expression in neurons and glial cells of layers II–VI. As this *in vivo* electroporation damaged brain tissue under the cathode plate, for this analysis we chose regions in which there were neither apoptotic nor necrotic cells in the electroporated tissues (Fig. 4). As a positive control for the TUNEL method we used brain tissues damaged with a surgical knife. In the control sections, apoptotic cells were observed (Fig. 4A–C), while there were no apoptotic cells in the neighbouring sections subjected to the morphological analysis of astrocytes (Fig. 4G–N). At the same

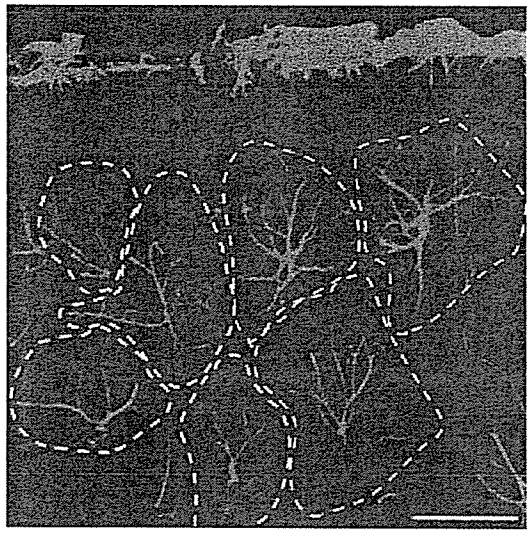

FIG. 2. Individual domains of layer I fibrous astrocytes. Astrocytes were visualized with anti-GFAP (green). The white dotted lines indicate the domain of each layer I fibrous astrocyte. Note that layer I fibrous astrocytes have separate domains, suggesting that we can observe the fine structures of astrocytes, such as processes and branching, without the problems of intermingling. Scale bar, 25 μm.

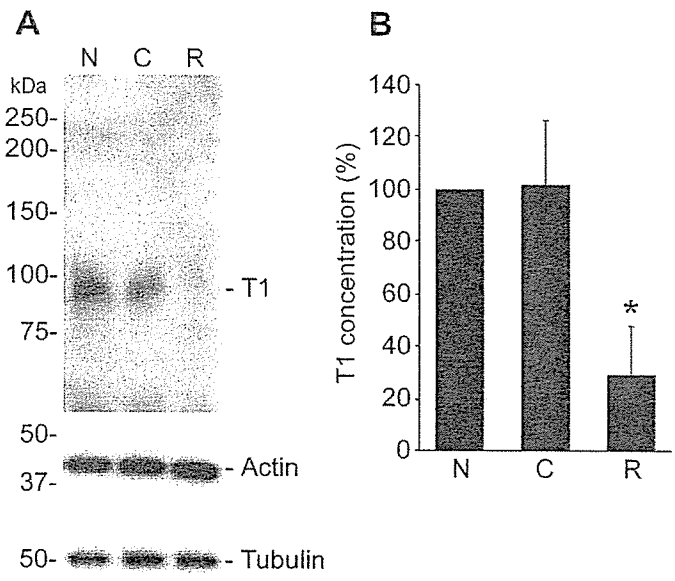

FIG. 3. Effect of T1 siRNA on T1 expression in C6 cells. (A) Either control vectors or T1 siRNA-expression vectors were transfected into C6 cells that intrinsically express T1. The expression of T1 was examined by Western blot analysis with anti-T1. The molecular weight of T1 was 95 kDa. The positions of the molecular weight markers are shown on the left. (B) Quantitative analysis of T1 bands in A. The expression level of T1 in the no transfection sample was taken as 100%. $*P < 0.05$ (one-way ANOVA) compared to the level of the no transfection sample. Values are given as means ± SD and were obtained from three independent experiments, and a representative image is shown. N, no transfection; C, control vector; R, siRNA vector.

time we assumed that the T1 siRNA-expression vector had been transferred into the astrocytes; this assumption was based on the expression of GFP, the expression vector of which was cotransferred with the siRNA vectors. In addition, it was observed that the GFP-expressing astrocytes did show a reduction in the T1 expression level (panel T1 in Fig. 5A).

To determine the *in vivo* efficiency of T1 siRNA, the quantitative analysis of *in vivo* T1 expression in the control- or siRNA-vector electroporated astrocytes was performed by measuring the fluorescent intensity of T1. The fluorescent intensity of T1 in the siRNA vector-electroporated astrocytes was significantly decreased compared with that in the control vector-electroporated astrocytes (Fig. 5C). Therefore, based on T1 expression, the siRNA vector was effective.

In the slices prepared from control vector-electroporated rats, BDNF induced a significant increment in the length and number of branches of the processes, while no change in primary process number was observed (Fig. 5). These amounts of change were identical to those observed in the nonelectroporated slices (Figs 1 and 5). When not treated with BDNF, slices prepared from the T1 siRNA vector-electroporated rats showed no difference from those with control vectors. Also, the astrocytes containing T1 siRNA-expression vectors appeared to have fewer branches and shorter processes under the no-BDNF treatment condition, though this difference was not significant (Fig. 5B). This result might be caused by an increase in cytosolic Rho GTPases due to the reduced expression of T1, which might bind and retain Rho GDI1 in the cell membrane. When treated with BDNF and inhibited T1 expression, astrocytes exhibited slight, albeit not significant, elongation and branching of the processes (Fig. 5B). These slight increases in process length and branching might be due to the low level of T1.

Relationship of GFAP$^+$ processes and synaptophysin$^+$ sites

Morphological changes in astrocytes have effects on the clearance of neurotransmitters and the regulation of synaptic transmission (Theodosis & Poulain, 1993; Iino *et al.*, 2001; Oliet *et al.*, 2001; Theodosis *et al.*, 2004). Moreover, in the cerebellum, Bergmann glial cells receive glutamate via ectopic release, and functional AMPA receptors are densely distributed in the Bergmann glial membrane that faces the synaptic structures (Matsui *et al.*, 2005), suggesting that astrocytic processes in close proximity to synapses may be capable of locally regulating synaptic functions. Thus, in this study we also addressed the question of whether or not the BDNF–T1 signalling leads to an increase in the number of synapses that are in contact with GFAP$^+$ processes. In this analysis, there is the possibility that synaptophysin$^+$ sites might represent cut axonal fibres. We assessed this problem using YFP-transgenic mice. In these mouse brains, YFP proteins were strongly expressed in the cell body, axons and dendrites of the layer V pyramidal neurons (Feng *et al.*, 2000). If cut axonal fibre terminals (YFP$^+$) were also synaptophysin$^+$, we would have detected the synaptophysin and YFP double-positive sites. However, we hardly found any such double-positive sites. Therefore, we considered synaptophysin$^+$ sites to be actual mature synapses (Okabe *et al.*, 2001). As shown in Fig. 6A and C, the number of synaptophysin$^+$ sites in contact with GFAP$^+$ processes increased in a BDNF-dependent manner, presumably because of the BDNF-induced extension of the astrocytic processes and astrocytic branching. On the other hand, neither BDNF nor NGF treatment was found to influence the overall density of synaptophysin$^+$ sites (Fig. 6D).

Next, we examined the effect of T1 siRNA on the interaction between GFAP$^+$ processes and synaptophysin$^+$ sites. In the control vector-electroporated slices, the number of synaptophysin$^+$ sites that were in contact with GFAP$^+$ processes increased more than two-fold, a result which was compatible with the amounts in the nonelectroporated slices (Fig. 6C). In contrast, no morphological changes among the astrocytes were observed in the T1 siRNA-expression vector electroporated slices. Moreover, the reduction in the number of synaptophysin$^+$ sites in contact with GFAP$^+$ processes appeared to

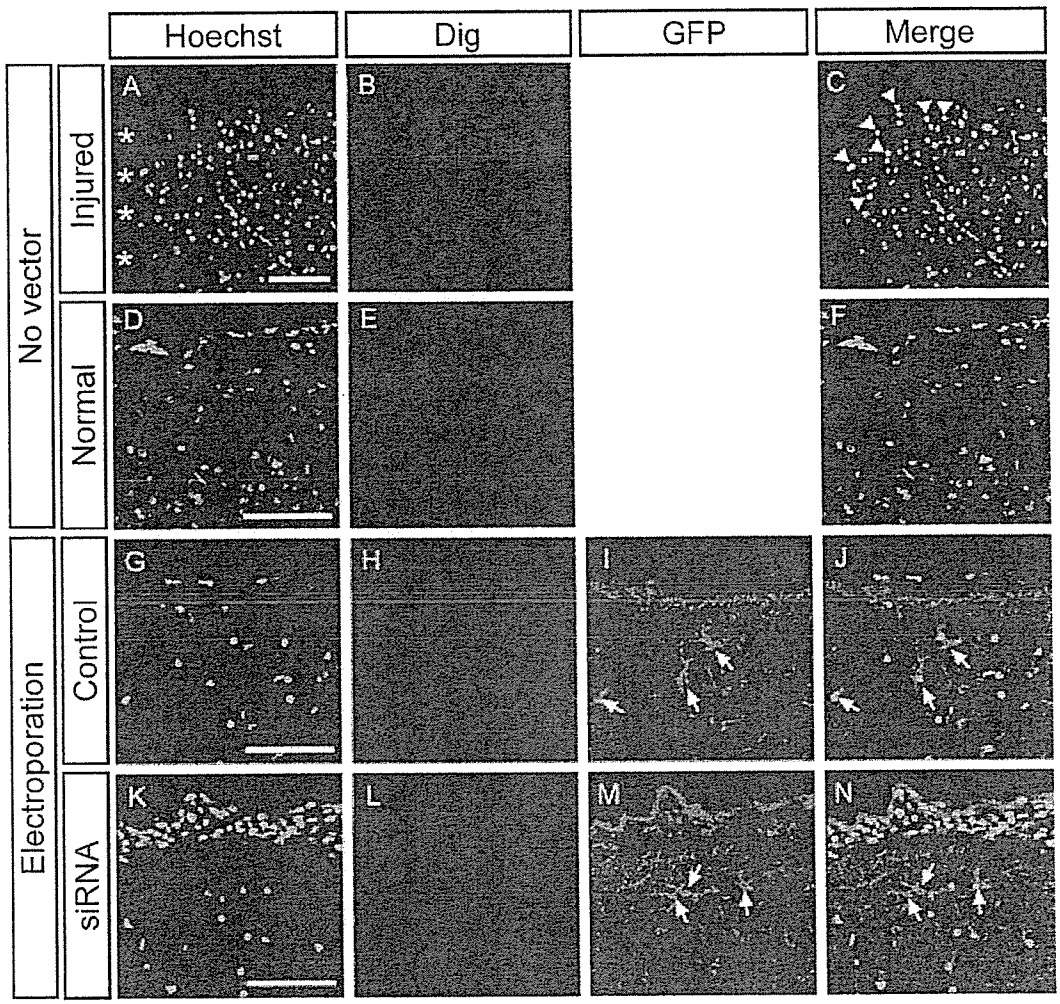

FIG. 4. Apoptotic cells in (A–C) injured, (D–F) unelectroporated, (G–J) control vector-electroporated, and (K–N) T1 siRNA vector-electroporated slices of the motor cortex. Apoptotic cells were detected by the TUNEL method with anti-Dig (B, E, H and L; red) and these cells are indicated by arrowheads. Electroporated cells expressed GFP (I and M; green cells indicated by arrows). Nuclei were stained with Hoechst 33258 (A, D, G, and K; blue). Note that the apoptotic cells, indicated by the arrowheads in C, were distributed around the injured region (asterisks in A), but were hardly detected in (E) the normal slices and in (H and L) the electroporated slices, thus suggesting that in these regions electroporation successfully delivered the plasmid vectors into neocortical layer I without inducing cell death. Scale bars, 100 μm.

reflect a decrease in $GFAP^+$ process length and in the branching induced by T1 siRNA, although this result was not significant (Fig. 6C).

Discussion

In this study, we demonstrated that BDNF regulated astrocytic morphology in adult neocortical slices via a truncated TrkB receptor, T1. Our data also revealed that the number of $synaptophysin^+$ sites in contact with $GFAP^+$ processes increased in a BDNF–T1-dependent manner without a change in the number of total $synaptophysin^+$ sites. Therefore, these results show that the neocortical layer I astrocytes exhibit high morphological plasticity in the adult rat brain.

Knock-down of T1 expression by siRNA and electroporation

In the present study, we performed *in vivo* knock-down of T1 by using T1 siRNA. The *trkB* gene contains at least three subtypes that have in common an extracellular domain, a transmembrane domain and the first 12 intracellular amino acid sequences. We designed the 19-mer oligonucleotide from adenosine at 1852 in the T1 sequence (GenBank accession number M55292). Interestingly, the control sequence started four nucleotides upstream of the T1 siRNA sequence. This control vector had virtually no RNAi effect on T1 expression (Fig. 3) or morphological changes in astrocytes (Figs 5 and 6), which was similar to the data from the normal rats (Figs 1 and 6). Although the cause was unknown, there was no great difference between the percentages of GC content in the two sequences. Thus, the secondary and/or tertiary structure of the resulting RNA might be the reason.

In this study, we performed electroporation to transfect the T1 siRNA-expression vectors into astrocytes. However, the electroporation and the cutting of slices kill the cells or weaken them. To choose the healthy areas in the slices, we checked the adjacent sections by the TUNEL method, which detects apoptotic cells. Also, we found gliosis as well as apoptosis at the margins of the areas damaged by electroporation. However, there was no gliosis in other areas (data not shown), because the electroporation of weak electric potential used in this study (five pulses of 50 ms, 15 V at 950-ms intervals) would cause limited focal damage, as reported in the previous studies (Kondoh *et al.*, 2000; Kachi *et al.*, 2005). Moreover, in the control vector-electroporated slices, the morphology of astrocytes (length,

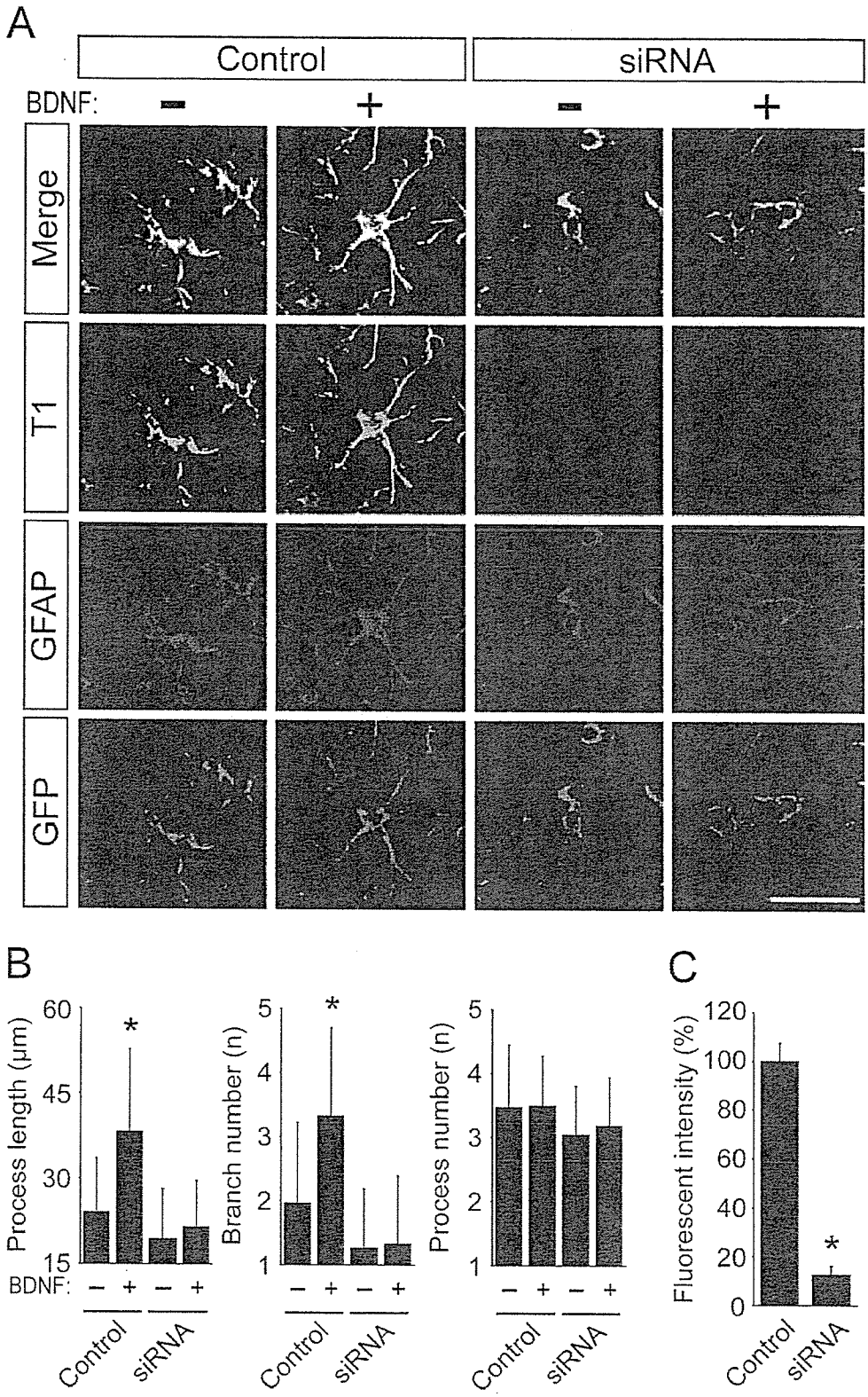

FIG. 5. Morphological changes in astrocytes transfected with T1 siRNA-expression vector. (A) Control or T1 siRNA-expression vector-electroporated astrocytes were visualized with anti-T1 (blue), anti-GFAP (red) and electroporated GFP (green). Slices were incubated for 60 min with BDNF (20 ng/mL) or vehicle (DMEM). Note that few T1-immunoreactive structures were observed in the T1 siRNA-expression vector-electroporated cells. (B) Quantitative analyses of process length (left panel), number of branches (middle panel) and number of processes (right panel). Values are given as means ± SD and are the results of four independent experiments. $*P < 0.05$ (two-way ANOVA) compared to astrocytes in the control slices not treated with BDNF. There was a significant difference in the BDNF treatment, but not a difference between the control- and the siRNA-expression vectors. (C) Quantitative analysis of T1 fluorescence intensity. Fluorescence intensity was measured with ImageJ. The expression level of T1 in the no transfection sample was taken as 100%. Values are given as means ± SD and are the results of four independent experiments. $*P < 0.05$, Student's *t*-test, between the T1 fluorescence intensity levels of the control and siRNA-expression vector transfected astrocytes. Control, electroporation of control vector; siRNA, electroporation of T1 siRNA-expression vector, –, no stimulation; +, stimulation with BDNF. Scale bar, 20 μm.

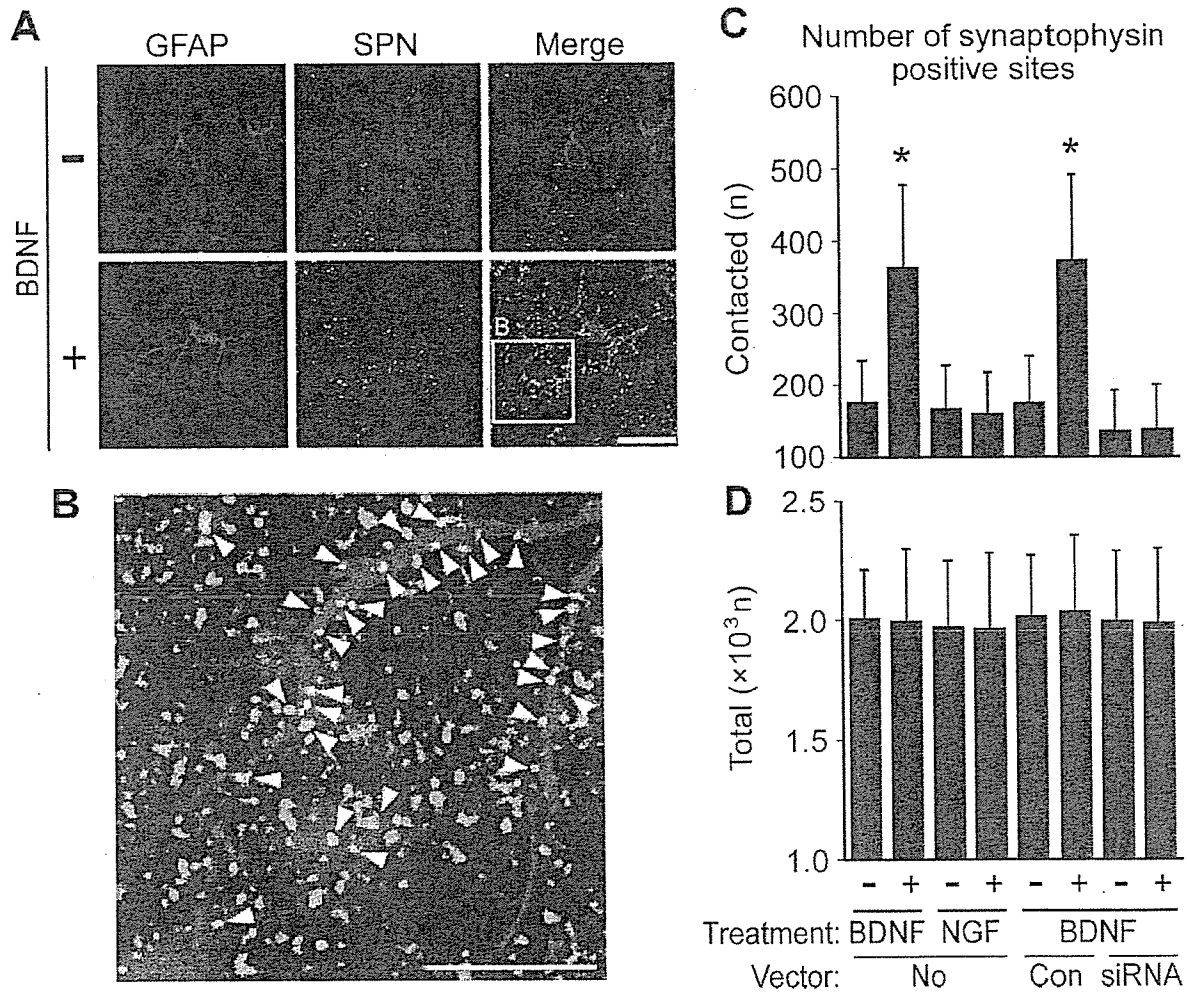

FIG. 6. Interaction between GFAP$^+$ processes and synaptophysin$^+$ sites. (A) Images of GFAP$^+$ processes (red) and synaptophysin (SPN)$^+$ sites (blue) in layer I of the motor cortex of normal acute slices. Slices were incubated for 60 min with BDNF (20 ng/mL) or vehicle (DMEM). (B) A high-powered image of the boxed-in area in A. Arrowheads indicate SPN$^+$ sites (white) in contact with GFAP$^+$ processes. (C and D) Quantitative analysis of (C) SPN$^+$ sites (white) in contact with GFAP$^+$ processes and (D) total SPN$^+$ sites. The normal slices, the control vector-electroporated slices and the RNAi vector-electroporated slices were treated with the indicated reagents: NGF (100 ng/mL), BDNF (20 ng/mL) and vehicle (DMEM). Values are given as means ± SD and are the results of four independent experiments. *$P < 0.05$ (one-way ANOVA and Scheffé's *post hoc* test) compared to the levels observed in astrocytes in normal slices not treated with BDNF; –, no stimulation; +, stimulation with NGF or BDNF. Scale bars, 20 μm.

branching and number of processes) was similar to that from the nontreated slices. Therefore, the morphology of astrocytes in the analysed areas was not affected by electroporation.

Subcellular localization of T1 and GFAP

The subcellular localization of T1 was very similar to that of GFAP (Figs 1 and 5). The single staining for T1 shows a uniform distribution of T1 in cell bodies and processes (Ohira *et al.*, 2005b). On the other hand, GFAP was also uniformly localized in the astrocytic cell bodies and processes (Fig. 2), suggesting that each specific antibody used here is not cross-reactive. Thus, these results indicate that proteins of both T1 and GFAP were distributed close to each other in astrocytes.

The colocalization of T1 and GFAP may indicate that T1 interacts with GFAP. In a previous study, we reported that T1 binds directly Rho GDI1, which is a negative regulator of a small G-protein family, Rho (Ohira *et al.*, 2005a). Additionally, T1 downregulates the activity of ROCK, a downstream effector kinase of RhoA, in a BDNF-dependent manner (Ohira *et al.*, 2006). Moreover, ROCK phosphorylates GFAP, which causes depolymerization of GFAP (Kosako *et al.*, 1997). Thus, T1 can regulate GFAP assembly via the Rho signalling pathway. Interestingly, all Trk family proteins can directly interact with an intermediate filament, peripherin (MacDonald *et al.*, 1999). All together, neurotrophins may be involved in regulation of cell morphology via cytoskeletal proteins such as intermediate filaments as well as microfilaments and microtubules (Etienne-Manneville & Hall, 2002).

Regulation of astrocytic morphology by BDNF–T1

In the adult mammalian CNS, BDNF is synthesized and secreted from pre- and postsynaptic neurons in a manner that depends on neuronal activity (Fawcett *et al.*, 1997, 1998; Aloyz *et al.*, 1999; Hartmann *et al.*, 2001; Kohara *et al.*, 2001). However, the physiological function of BDNF in the adult CNS remains unclear. One of the reasons that the function of BDNF in the adult mammalian CNS has not yet been clarified is that the function of T1, the major receptor for BDNF in the adult mammalian CNS from mice to nonhuman primates, has yet to be

addressed (Allendoerfer *et al.*, 1994; Fryer *et al.*, 1996; Ohira *et al.*, 1999). In the adult monkey prefrontal cortex, TK+/TK– heterodimers and TK–/TK– homodimers are formed in a BDNF-dependent manner; however, TK+/TK+ homodimers that function during development are not observed (Ohira *et al.*, 2001). These lines of evidence suggested that TK– (i.e. T1 in the adult neocortex) plays an important role in the maintenance and plasticity of the adult neocortex. Indeed, recent studies have demonstrated the function and signalling pathway of T1 (Rose *et al.*, 2003; Ohira *et al.*, 2005a; Ohira *et al.*, 2006). Thus, these studies provide clues to the elucidation of *in vivo* function of BDNF in the mature CNS.

T1 is expressed in both neurons and glial cells (Armanini *et al.*, 1995; Ohira *et al.*, 2005b), and it is highly involved in the regulation of the morphology of both types of cell (Yacoubian & Lo, 2000; Ohira *et al.*, 2005a). In terms of function, glial cells, and especially astrocytes, have been thought to play only a supportive role for neurons. However, recent studies have demonstrated that glial cells regulate the clearance of neurotransmitters, and that they maintain neural plasticity by themselves undergoing morphological changes (Theodosis & Poulain, 1993; Iino *et al.*, 2001; Oliet *et al.*, 2001; Theodosis *et al.*, 2004). In contrast, neuronal morphology in the adult rodent neocortex has been shown to be more static than previously thought (Grutzendler *et al.*, 2002). The findings of the present study are thus consistent with these previous findings. In the adult CNS, BDNF release might induce morphological changes in those astrocytic processes surrounding synapses via the T1 signalling pathway, eventually leading to rapid changes in synaptic strength and transmission (Wenzel *et al.*, 1991). However, it remains unclear whether or not the site-specific release of BDNF regulates astrocytic morphology and affects synaptic transmission and plasticity *in vivo* as well as in tissue slices.

It is reasonable to expect that BDNF treatment induces neurons to release factors that in turn regulate astrocytic morphology. In this study, we did not directly test this possibility. However, considering that (i) T1 regulates astrocytic morphology in astrocyte primary cultures in which the *in vivo* expression pattern of BDNF receptors is maintained (Ohira *et al.*, 2005a), and (ii) T1-specific siRNA electroporated into astrocytes suppressed BDNF-induced morphological changes in astrocytes, we concluded that the astrocytic morphology in the acute slices observed here was regulated by the BDNF–T1 signalling pathway in the astrocytes themselves.

In the present study, $GFAP^+$ astrocytic processes exhibited BDNF-dependent elongation of up to 15 μm, whereas previous studies have reported changes in process length of only several micrometers in the astrocytes of the brainstem (Hirrlinger *et al.*, 2004) and hippocampus (Benediktsson *et al.*, 2005). Previous reports have noted the spontaneous elongation and retraction of fine processes of protoplasmic astrocytes, in which glutamate, ATP and other factors would be expected to be involved in the regulation of astrocytic morphology (Volterra & Meldolesi, 2005). As *in vivo* BDNF release from synapses is regulated by neuronal activity, a bath application of BDNF would be expected to continuously stimulate astrocytes and result in a stronger elongation and branching effect among astrocytic processes. However, this effect may also reflect a difference between protoplasmic and fibrous astrocytes.

Functional significance of BDNF–T1 in neocortical layer I astrocytes

It is of note that, in the adult rat neocortex, the strongest BDNF immunoreactivity is observed in layer I (Yan *et al.*, 1997), which suggests that BDNF is enriched and functions in neocortical layer I. Neocortical layer I contains a small number of neurons and is composed predominantly of dendritic and axonal connections (Lund & Wu, 1997) which receive feedback inputs from the cortex (Rockland & Virga, 1989) and inputs from the thalamic nuclei (Glenn *et al.*, 1982; Lachica & Casagrande, 1992) as well as from other subcortical regions (Tigges & Tigges, 1985). The apical dendrites of pyramidal neurons in layers II–VI reach layer I (Lund & Wu, 1997). Thus, layer I is an important region in which the feedforward and feedback information from higher cortical areas, as well as from other lower cortical areas and subcortical regions, could be associated (Zhu & Zhu, 2004). Moreover, neocortical layer I is a network layer which would exert a direct and concerted effect on the firing properties of pyramidal cells in the deep layers (Chu *et al.*, 2003; Shlosberg *et al.*, 2003). In this context, one might consider whether or not the spillover of BDNF from a certain active synapse would affect the neighbouring inactive synapses. If so, the entanglement of neuronal wires would ensue, which would be quite detrimental to neuronal function. Therefore, in order to block the leakage of neurotransmitters and other functional molecules, as well as that of BDNF, from active synapses, the astrocytes that surround active synapses may alter their morphology in response to a spillover of BDNF; in this case, astrocytes could be considered an 'insulator' of synapses. At the same time, these morphological changes among astrocytes may regulate synaptic transmission in active synapses via the release of neurotransmitters from the astrocytes themselves; in this case, astrocytes would act as an 'amplifier' of transmission (Bezzi *et al.*, 2004; Fiacco & McCarthy, 2004).

Implications of T1 and morphological changes among astrocytes and neurons in terms of adult neural plasticity

According to the current paradigm, long-term morphological changes among neurons are fundamental to learning and memory. In the present model there exists a possible mechanism for the morphological alteration of neurons and astrocytes in which BDNF–T1 signalling may also be involved.

Long-term changes in glial processes in the living brain may exert an influence on neuronal morphology. For example, the adult hypothalamo-neurohypophysial system undergoes activity-dependent morphological plasticity which modifies astrocytic coverage of its oxytocinergic neurons and their synaptic inputs. Interestingly, reduced coverage of astrocytes at synaptic sites can be maintained for 1 month by lactation (Theodosis & Poulain, 1993; Theodosis *et al.*, 2004); this finding suggests that continuous neuronal stimulation can alter as well as maintain glial morphology. In addition, such glial changes can induce morphological changes in synapses (Theodosis & Poulain, 1993; Theodosis *et al.*, 2004). In other words, a prior morphological change in the glial cells might orientate neurons with respect to sites for dendrite elongation and synapse formation. Additional studies will be needed to further clarify the changes in neuronal fine structures.

Acknowledgements

We would like to thank Dr Hans Thoenen for his helpful suggestions and comments, Dr Keiji Wada for the gift of YFP transgenic mice, and Ms Tomoko Kohno, Ms Mikako Sakurai and Ms Hiromi Fujita for genotyping of YFP mice. This work was supported by grants from the Ministry of Education, Culture, Sports, Science and Technology of Japan [no. 18700343 to K.O., no. 15016056 to M.H., nos 16200025, 17022020 and 17650100 to T.K., no. 16015341 to S.N., the Biodiversity Research of 21st Century COE (A14)] and the Organization of Pharmaceutical Safety and Research (nano-1), a Sasakawa Scientific Research Grant from The Japan Science Society, and a Core Research for Evolutional Science and Technology (CREST) grant from the Japan Science and Technology Agency (JST).

Abbreviations

BDNF, brain-derived neurotrophic factor; GFAP, glial fibrillary acidic protein; GFP, green fluorescent protein; NGF, nerve growth factor; NT, neurotrophin; S-D, Sprague–Dawley; siRNA, small interfering RNA; TrkB, tropomyosin-related kinase B; TUNEL, terminal deoxynucleotidyl transferase-mediated digoxigenin nucleotide nick-end labelling; YFP, yellow fluorescent protein.

References

Allendoerfer, K.L., Cabelli, R.J., Escanòn, E., Kaplan, D.R., Nikolics, K. & Shatz, C.J. (1994) Regulation of neurotrophin receptors during the maturation of the mammalian visual system. *J. Neurosci.*, **14**, 1795–1811.

Aloyz, R., Fawcett, J.P., Kaplan, D.R., Murphy, R.A. & Miller, F.D. (1999) Activity-dependent activation of TrkB neurotrophin receptors in the adult CNS. *Learn. Mem.*, **6**, 216–231.

Araque, A., Parpura, V., Sanzgiri, R.P. & Haydon, P.G. (2001) Tripartite synapses: glia, the unacknowledged partner. *Trends Neurosci.*, **22**, 208–215.

Armanini, M.P., McMahon, S.B., Sutherland, J., Shelton, D.L. & Phillips, H.S. (1995) Truncated and catalytic isoforms of trkB are co-expressed in neurons of rat and mouse CNS. *Eur. J. Neurosci.*, **7**, 1403–1409.

Barbacid, M. (1994) The Trk family of neurotrophin receptors. *J. Neurobiol.*, **25**, 1386–1403.

Benediktsson, A.M., Schachtele, S.J., Green, S.H. & Dailey, M.E. (2005) Ballistic labeling and dynamic imaging of astrocytes in organotypic hippocampal slice cultures. *J. Neurosci. Meth.*, **141**, 41–53.

Bezzi, P., Gundersen, V., Galbete, J.L., Seifert, G., Steinhauser, C., Pilati, E. & Volterra, A. (2004) Astrocytes contain a vesicular compartment that is competent for regulated exocytosis of glutamate. *Nat. Neurosci.*, **7**, 613–620.

Bibel, M. & Barde, Y.A. (2000) Neurotrophins: key regulators of cell fate and cell shapes in the vertebrate nervous system. *Genes Dev.*, **14**, 2919–2937.

Bushong, E.A., Martone, M.E., Jones, Y.Z. & Ellisman, M.H. (2002) Protoplasmic astrocytes in CA1 striatum radiatum occupy separate anatomical domains. *J. Neurosci.*, **22**, 183–192.

Chu, Z., Galarreta, M. & Hestrin, S. (2003) Synaptic interactions of late-spiking neocortical neurons in layer 1. *J. Neurosci.*, **23**, 96–102.

Colombo, J.A., Fuchs, E., Härtig, W., Marotte, L.R. & Puissant, V. (2000) 'Rodent-like' and 'primate-like' types of astroglial architecture in the adult cerebral cortex of mammals: a comparative study. *Anat. Embryol.*, **201**, 111–120.

Etienne-Manneville, S. & Hall, A. (2002) Rho GTPases in cell biology. *Nature*, **420**, 629–635.

Fawcett, J.P., Aloyz, R., McLean, J.H., Pareek, S., Miller, F.D., McPherson, P.S. & Murphy, R.A. (1997) Detection of brain-derived neurotrophic factor in a vesicular fraction of brain synaptosomes. *J. Biol. Chem.*, **272**, 8837–8840.

Fawcett, J.P., Bamji, S.X., Causing, C.G., Aloyz, R., Ase, A.R., Reader, T.A., McLean, J.H. & Miller, F.D. (1998) Functional evidence that BDNF is an anterograde neuronal trophic factor in the CNS. *J. Neurosci.*, **18**, 2808–2821.

Fellin, T. & Carmignoto, G. (2004) Neurone-to-astrocyte signalling in the brain represents a distinct multifunctional unit. *J. Physiol. (Lond.)*, **559**, 3–15.

Feng, G., Mellor, R.H., Bernstein, M., Keller-Peck, C., Nguyen, Q.T., Wallace, M., Nerbonne, J.M., Lichtman, J.W. & Sanes, J.R. (2000) Imaging neuronal subsets in transgenic mice expressing multiple spectral variants of GFP. *Neuron*, **28**, 41–51.

Fiacco, T.A. & McCarthy, K.D. (2004) Intracellular astrocyte calcium waves in situ increase the frequency of spontaneous AMPA receptor currents in CA1 pyramidal neurons. *J. Neurosci.*, **24**, 722–732.

Fryer, R.H., Kaplan, D.R., Feinstein, S.C., Radeke, M.J., Grayson, D.R. & Kromer, L.F. (1996) Developmental and mature expression of full-length and truncated TrkB receptors in the rat forebrain. *J. Comp. Neurol.*, **374**, 21–40.

Glenn, L.L., Hada, J., Roy, J.P., Deschênes, M. & Steriade, M. (1982) Anterograde tracer and field potential analysis of the neocortical layer I projection from nucleus ventralis medialis of the thalamus in cat. *Neuroscience*, **7**, 1861–1877.

Grutzendler, J., Kasthuri, N. & Gan, W.B. (2002) Long-term dendritic spine stability in the adult cortex. *Nature*, **420**, 812–816.

Hartmann, M., Heumann, R. & Lessmann, V. (2001) Synaptic secretion of BDNF after high-frequency stimulation of glutamatergic synapses. *EMBO J.*, **20**, 5887–5897.

Hirrlinger, J., Hülsmann, S. & Kirchhoff, F. (2004) Astroglial processes show spontaneous motility at active synaptic terminals in situ. *Eur. J. Neurosci.*, **20**, 2235–2239.

Iino, M., Goto, K., Kakegawa, W., Okado, H., Sudo, M., Ishiuchi, S., Miwa, A., Takayasu, Y., Saito, I., Tsuzuki, K. & Ozawa, S. (2001) Glia–synapse interaction through Ca^{2+}-permeable AMPA receptors in Bergmann glia. *Science*, **292**, 926–929.

Kachi, S., Oshima, Y., Esumi, N., Kachi, M., Zack, D.J. & Campochiaro, P.A. (2005) Nonviral ocular gene transfer. *Gene Ther.*, **12**, 843–851.

Klein, R., Conway, D., Parada, L.F. & Barbacid, M. (1990) The trkB tyrosine kinase gene codes for a second neurogenic receptor that lacks the catalytic kinase domain. *Cell*, **61**, 647–656.

Kohara, K., Kitamura, A., Morishima, M. & Tsumoto, T. (2001) Activity-dependent transfer of brain-derived neurotrophic factor to postsynaptic neurons. *Science*, **291**, 2419–2423.

Kondoh, T., Motooka, Y., Bhattacharjee, A.K., Kokunai, T., Saito, N. & Tamaki, N. (2000) In vivo gene transfer into the periventricular region by electroporation. *Neurol. Med. Chir. (Tokyo)*, **40**, 618–623.

Kosako, H., Amano, M., Yanagida, M., Tanabe, K., Nishi, Y., Kaibuchi, K. & Inagaki, M. (1997) Phosphorylation of glial fibrillary acidic protein at the same sites by cleavage furrow kinase and Rho-associated kinase. *J. Biol. Chem.*, **272**, 10333–10336.

Lachica, E.A. & Casagrande, V.A. (1992) Direct W-like geniculate projections to the cytochrome oxidase (CO) blobs in primate visual cortex: axon morphology. *J. Comp. Neurol.*, **319**, 141–158.

Langle, S.L., Poulain, D.A. & Theodosis, D.T. (2003) Induction of rapid, activity-dependent neuronal-glial remodeling in the adult rat hypothalamus *in vitro*. *Eur. J. Neurosci.*, **18**, 206–214.

Lund, J.S. & Wu, C.Q. (1997) Local circuit neurons of macaque monkey striate cortex. IV. Neurons of laminae 1–3A. *J. Comp. Neurol.*, **384**, 109–126.

MacDonald, J.I.S., Verdi, J.M. & Meakin, S.O. (1999) Activity-dependent interaction of the intercellular domain of rat TrkA with intermediate filament proteins, the β-6 proteasomal subunit, Ras-GRF1, and the p162 subunit of eIF3. *J. Mol. Neurosci.*, **13**, 141–158.

Matsui, K., Jahr, C.E. & Rubio, M.E. (2005) High-concentration rapid transients of glutamate mediate neural-glial communication via ectopic release. *J. Neurosci.*, **25**, 7538–7547.

Middlemas, D.S., Lindberg, R.A. & Hunter, T. (1991) trkB, a neural receptor protein-tyrosine kinase: evidence for a full-length and two truncated receptors. *Mol. Cell. Biol.*, **11**, 143–153.

Miller, R.H. & Raff, M.C. (1984) Fibrous and protoplasmic astrocytes are Biochemically and developmentally distinct. *J. Neurosci.*, **4**, 585–592.

Ohira, K., Funatsu, N., Nakamura, S. & Hayashi, M. (2004) Expression of BDNF and TrkB receptor subtypes in the postnatal developing Purkinje cells of monkey cerebellum. *Gene Expr. Patterns*, **4**, 257–261.

Ohira, K. & Hayashi, M. (2003) Expression of TrkB subtypes in the adult monkey cerebellar cortex. *J. Chem. Neuroanat.*, **25**, 175–183.

Ohira, K., Homma, K.J., Hirai, H., Nakamura, S. & Hayashi, M. (2006) TrkB-T1 Regulates the RhoA signaling and actin cytoskeleton in glioma cells. *Biochem. Biophys. Res. Commun.*, **342**, 867–874.

Ohira, K., Kumanogoh, H., Sahara, Y., Homma, K.J., Hirai, H., Nakamura, S. & Hayashi, M. (2005a) A truncated tropo-myosine-related kinase B receptor, T1, regulates glial cell morphology via Rho GDP dissociation inhibitor 1. *J. Neurosci.*, **25**, 1343–1353.

Ohira, K., Shimizu, K. & Hayashi, M. (1999) Change of expression of full-length and truncated TrkBs in the developing monkey central nervous system. *Dev. Brain Res.*, **112**, 21–29.

Ohira, K., Shimizu, K. & Hayashi, M. (2001) TrkB dimerization during development of the prefrontal cortex of the macaque. *J. Neurosci. Res.*, **65**, 463–469.

Ohira, K., Shimizu, K., Yamashita, A. & Hayashi, M. (2005b) Differential expression of the truncated TrkB receptor, T1, in the primary motor and prefrontal cortices of the adult macaque monkey. *Neurosci. Lett.*, **385**, 105–109.

Okabe, S., Miwa, A. & Okado, H. (2001) Spine formation and correlated assembly of presynaptic and postsynaptic molecules. *J. Neurosci.*, **21**, 6105–6114.

Oliet, S.H., Piet, R. & Poulain, D.A. (2001) Control of glutamate clearance and synaptic efficacy by glial coverage of neurons. *Science*, **292**, 923–926.

Paxinos, G. & Watson, C. (1986) The rat brain in stereotaxic coordinates, 2nd Edn. Academic Press, San Diego.

Peters, A., Palay, S.L., de Webster, H. & F. (1976) *The Fine Structure of the Nervous System: the Neurons and Supporting Cells*. W.B. Saunders Co., Philadelphia, pp. 242–244.

Raff, M.C., Abney, E.R., Cohen, J., Lindsay, R. & Noble, M. (1983) Two types of astrocytes in cultures of developing rat white matter: differences in morphology, surface gangliosides, and growth characteristics. *J. Neurosci.*, **3**, 1289–1300.

Rockland, K.S. & Virga, A. (1989) Terminal arbors of individual 'feedback' axons projecting from area V2 to V1 in the macaque monkey: a study using

immunohistochemistry of anterogradely transported Phaseolus vulgaris-leucoagglutinin. *J. Comp. Neurol.*, **285**, 54–72.

Rose, C.R., Blum, R., Pichler, B., Lepier, A., Kafitz, K.W. & Konnerth, A. (2003) Truncated TrkB-T1 mediates neurotrophin-evoked calcium signalling in glia cells. *Nature*, **426**, 74–78.

Shlosberg, D., Patrick, S.L., Buskila, Y. & Amitai, Y. (2003) Inhibitory effect of mouse neocortex layer I on the underlying cellular network. *Eur. J. Neurosci.*, **18**, 2751–2759.

Theodosis, D.T., Piet, R., Poulain, D.A. & Oliet, S.H.R. (2004) Neuronal, glial and synaptic remodeling in the adult hypothalamus: functional consequences and role of cell surface and extracellular matrix adhesion molecules. *Neurochem. Int.*, **45**, 491–501.

Theodosis, D.T. & Poulain, D.A. (1993) Activity-dependent neuronal-glial and synaptic plasticity in the adult mammalian hypothalamus. *Neuroscience*, **57**, 501–535.

Tigges, J. & Tigges, M. (1985) Subcortical sources of direct projections to visual cortex. In Peters, A. & Jones, E.G. (eds), *Cerebral Cortex: Visual Cortex*, **Vol. 3**. Plenum Press, New York, pp. 351–378.

Ventura, R. & Harris, K.M. (1999) Three-dimensional relationships between hippocampal synapses and astrocytes. *J. Neurosci.*, **19**, 6897–6906.

Volterra, A. & Meldolest. J. (2005) Astrocytes, from brain glue to communication elements: the revolution continues. *Nat. Rev. Neurosci.*, **6**, 626–640.

Wenzel, J., Lammert, G., Meyer, U. & Krug, M. (1991) The influence of long-term potentiation on the spatial relationship between astrocyte processes and potentiated synapses in the dentate gyrus neuropil of rat brain. *Brain Res.*, **560**, 122–131.

Wiesenhofer, B., Kaufmann, W.A. & Humpel, C. (1999) Improved lipid-mediated gene transfer in C6 glioma cells and primary glial cells using FuGene. *J. Neurosci. Meth.*, **92**, 145–152.

Yacoubian, T.A. & Lo, D.C. (2000) Truncated and full-length TrkB receptors regulate distinct modes of dendritic growth. *Nat. Neurosci.*, **3**, 342–349.

Yan, Q., Rosenfeld, R.D., Matheson, C.R., Hawkins, N., Lopez, O.T., Bennett, L. & Welcher, A.A. (1997) Expression of brain-derived neurotrophic factor protein in the adult rat central nervous system. *Neuroscience*, **78**, 431–448.

Zhu, Y. & Zhu, J.J. (2004) Rapid arrival and integration of ascending sensory information in layer 1 nonpyramidal neurons and tuft dendrites of layer 5 pyramidal neurons of the neocortex. *J. Neurosci.*, **24**, 1272–1279.

Available online at www.sciencedirect.com
ScienceDirect
Neurochemistry International 50 (2007) 119–129
NEUROCHEMISTRY International
www.elsevier.com/locate/neuint

Dopaminergic neuronal loss in transgenic mice expressing the Parkinson's disease-associated UCH-L1 I93M mutant

Rieko Setsuie [a,b,1], Yu-Lai Wang [a,1], Hideki Mochizuki [c,d], Hitoshi Osaka [a,e], Hideki Hayakawa [c], Nobutsune Ichihara [f], Hang Li [a], Akiko Furuta [a], Yae Sano [a,b], Ying-Jie Sun [a], Jungkee Kwon [a,g], Tomohiro Kabuta [a], Kenji Yoshimi [d], Shunsuke Aoki [a], Yoshikuni Mizuno [c,d], Mami Noda [b], Keiji Wada [a,*]

[a] *Department of Degenerative Neurological Diseases, National Institute of Neuroscience, National Center of Neurology and Psychiatory, Kodaira, Tokyo 187-8502, Japan*
[b] *Laboratory of Pathophysiology, Graduate School of Pharmaceutical Sciences, Kyushu University, Higashi-ku, Fukuoka 812-8582, Japan*
[c] *Department of Neurology, Juntendo University School of Medicine, Bunkyo-ku, Tokyo 113-8421, Japan*
[d] *Research Institute for Diseases of Old Age, Juntendo University School of Medicine, Bunkyo-ku, Tokyo 113-8421, Japan*
[e] *Division of Neurology, Clinical Research Institute, Kanagawa Children's Medical Center, Yokohama 232-8555, Japan*
[f] *Department of Anatomy, School of Veterinary Medicine, Azabu University, Sagamihara 229-8501, Japan*
[g] *College of Veterinary Medicine, Chonbuk National University, 644-14 Duckjin-Ku, Jeonju 561-756, Republic of Korea*

Received 14 March 2006; received in revised form 19 June 2006; accepted 11 July 2006
Available online 11 September 2006

Abstract

The I93M mutation in ubiquitin carboxyl-terminal hydrolase L1 (UCH-L1) was reported in one German family with autosomal dominant Parkinson's disease (PD). The causative role of the mutation has, however, been questioned. We generated transgenic (Tg) mice carrying human *UCHL1* under control of the *PDGF-B* promoter; two independent lines were generated with the I93M mutation (a high- and low-expressing line) and one line with wild-type human UCH-L1. We found a significant reduction in the dopaminergic neurons in the substantia nigra and the dopamine content in the striatum in the high-expressing I93M Tg mice as compared with non-Tg mice at 20 weeks of age. Although these changes were absent in the low-expressing I93M Tg mice, 1-methyl-4-phenyl-1,2,3,6-tetrahydropyridine (MPTP) treatment profoundly reduced dopaminergic neurons in this line as compared with wild-type Tg or non-Tg mice. Abnormal neuropathologies were also observed, such as silver staining-positive argyrophilic grains in the perikarya of degenerating dopaminergic neurons, in I93M Tg mice. The midbrains of I93M Tg mice contained increased amounts of insoluble UCH-L1 as compared with those of non-Tg mice, perhaps resulting in a toxic gain of function. Collectively, our data represent *in vivo* evidence that expression of $UCHL1^{I93M}$ leads to the degeneration of dopaminergic neurons.

Keywords: Ubiquitin carboxy-terminal hydrolase L1; Animal model; Parkinson's disease; Dopaminergic neuron

1. Introduction

Parkinson's disease (PD) is the second most common human neurodegenerative disorder after Alzheimer's disease (AD) (Dauer and Przedborski, 2003; Vila and Przedborski, 2004). PD patients exhibit motor dysfunction, including slowed movement (bradykinesia), resting tremor, rigidity, and postural instability (Dauer and Przedborski, 2003). The pathological basis of PD is the progressive loss of dopaminergic neurons in the substantia nigra pars compacta, giving rise to a decrease in dopamine content in the striatum (Dauer and Przedborski, 2003). Although most cases of PD are sporadic, studies of familial PD have provided accumulating evidence for the molecular mechanisms of PD. Thus far, at least six proteins have been identified to cause familial PD: α-synuclein (Chartier-Harlin et al., 2004; Farrer et al., 2004; Ibanez et al., 2004; Kruger et al., 1998; Polymeropoulos et al., 1997; Singleton et al., 2003), UCH-L1 (Leroy et al., 1998), parkin (Kitada et al., 1998), DJ-1 (Bonifati et al., 2003), phosphatase

* Corresponding author. Tel.: +81 42 346 1715; fax: +81 42 346 1745.
E-mail address: wada@ncnp.go.jp (K. Wada).
[1] These authors contributed equally to this work.

0197-0186/$ – see front matter © 2006 Elsevier Ltd. All rights reserved.
doi:10.1016/j.neuint.2006.07.015

and tensin homolog induced kinase-1 (PINK1) (Valente et al., 2004), and leucine-rich repeat kinase-2 (LRRK2) (Paisan-Ruiz et al., 2004; Zimprich et al., 2004). α-Synuclein, UCH-L1 and LRRK2 are linked to the autosomal dominant form of PD, whereas parkin, DJ-1 and PINK1 are linked to the recessive form.

In 1998, UCH-L1 carrying an Ile to Met mutation at amino acid position 93 (I93M) was identified in one German family affected by autosomal dominant familial PD. UCH-L1, also known as PGP9.5, is an abundant protein in neuronal cells, comprising up to about 1–2% of total protein in the brain. Its function as de-ubiquitylating enzyme (Larsen et al., 1998; Wilkinson et al., 1989), ubiquitylating enzyme (Liu et al., 2002), de-neddylating enzyme (Hemelaar et al., 2004), and mono-ubiquitin stabilizer (Osaka et al., 2003) has been reported. *In vitro* analysis using recombinant human UCH-L1 indicated that I93M mutation results in the reduction of hydrolase activity of about 50% (Nishikawa et al., 2003). *Uchl1* gene deletion in mice, however, was reported to causes gracile axonal dystrophy (*gad*), a recessive neurodegenerative disease with distinct phenotype and pathological features from PD (Saigoh et al., 1999). Moreover, extensive analysis failed to find other PD patients with mutations in the *UCHL1* gene (Lincoln et al., 1999; Maraganore et al., 1999) and there was an incomplete penetrance in reported German family (Leroy et al., 1998). Thus, the correlation of I93M mutation and pathogenesis of PD was questioned.

To elucidate the pathological role of UCH-L1^{I93M} expression in the pathogenesis of PD, *in vivo*, we generated transgenic mice expressing human UCH-L1^{I93M}.

2. Experimental procedures

2.1. Generation of *hUCHL1*^{WT} and *hUCHL1*^{I93M} transgenic mice

We generated transgenes by cloning either the wild-type or I93M mutant human UCH-L1 cDNAs under the control of the human platelet-derived growth factor B chain (*PDGF-B*) promoter (Fig. 1A) (Sasahara et al., 1991). Sequences encoding *UCHL1* were amplified from a human brain cDNA library (Stratagene, La Jolla, CA) by PCR and subcloned into the *Xho*I and *Not*I sites of pCI-neo (Promega, Madison, WI). The I93M substitution was obtained using QuikChange (Stratagene). The 5′ flanking region of the human *PDGF-B* chain gene was isolated from the human genomic DNA and inserted into the *Bgl*II and *Xho*I site of pCI-neo which results in the replacement of promoter from CMV to *PDGF-B*. The plasmid was linearized by digestion with *Hin*dIII and *Aat*II. A 2 μg/ml solution of the linearized plasmid of each transgene was then microinjected into the pronuclei of newly fertilized C57BL/6J mouse eggs. Offspring were screened for the presence of the transgene by PCR of tail DNA using specific primers (forward: PD-UCH-2, 5′-GCACTCTCCCTTCTCCTTTATA-3′; reverse: PD-UCH-5, 5′-CCTGTATGGCCTCATTCTTTTC-3′). Expression of hUCH-L1^{I93M} in a low-expressing mouse line only occurred in male mice. Thus, all experiments were done using male heterozygous transgenic mice. Animal care and handling were in accordance with institutional regulations for animal care and were approved by the Animal Investigation Committee of the National Institute of Neuroscience, National Center of Neurology and Psychiatry, Tokyo, Japan which conforms the National Institute of Health guide for the care and use of Laboratory animals.

2.2. Quantitative RT-PCR analysis

Primers specific for mouse *Uchl1* (forward: mL1-7, 5′-CCTTGGTTTGCAG-CTTTAGCA-3′; reverse: mL1-8, 5′-GGGCTGTAGAACGCAAGAAGA-3′) and human *UCHL1* (forward: L1Tg-F2, 5′-TGGCAACTTCTCCTCCTGCA-3′; reverse: L1Tg-R2, 5′-ACAGCACTTTGTTCAGCATC-3′) were designed, and SYBR Green-based real-time quantitative RT-PCR was performed using the ABI PRISM 7700 (Applied Biosystems, Foster City, CA) using total RNA from mouse brain ($n = 3$ for each line) (Aoki et al., 2002). GAPDH was used as an internal control.

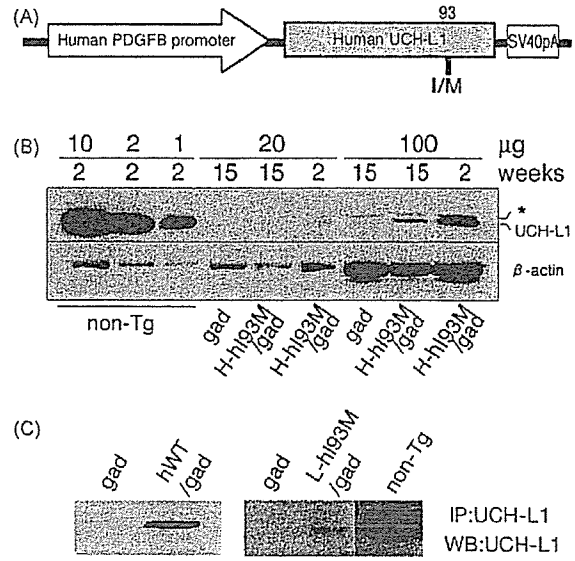

Fig. 1. Generation of transgenic mice expressing hUCH-L1^{WT} and hUCH-L1^{I93M}. (A) UCH-L1^{I93M} was constructed under control of the *PDGF-B* promoter, as depicted. (B) Immunoblotting analysis of endogenous mouse UCH-L1 and transgenic human UCH-L1 expression in mouse midbrain. To detect exogenous human UCH-L1 levels specifically, we generated transgenic mice in the *gad* background (H-hI93M/*gad*), which corresponds to the null mutant of *Uchl1*. Notice that the faint band corresponding to UCH-L1 is detected at 2 weeks of age when 20 μg protein/lane was loaded for the detergent-soluble fraction of midbrain origin in H-hI93M/*gad* mice. When the applied protein was increased to 100 μg/lane, UCH-L1 was easily detected at 2 weeks in H-hI93M/*gad* mice, and UCH-L1 levels markedly decreased by age 15 weeks. Faint bands indicated by the asterisk may correspond to UCH-L3, which cross-reacted with the UCH-L1 antibody when a large amount of protein was loaded per lane. (C) Immunoprecipitation analysis of exogenous human UCH-L1 in hWT/gad (left) and L-hI93M/gad (right) brains. Brain lysates from hWT/gad (left) or L-hI93M/gad (right) were both immunoprecipitated and detected using anti-UCH-L1 antibody. The band corresponding to the UCH-L1 can be found in both hWT/gad and L-hI93M/gad lysates but not in gad lysates indicating the exogenous human UCH-L1 expression.

2.3. Fractionation and immunoblotting and immunoprecipitation

For the immunoblotting of total UCH-L1, the soluble fraction in RIPA (20 mM Tris–HCl, pH 7.5; 0.1% SDS; 1.0% (w/v) Triton X-100; 1.0% sodium deoxycholate) with Complete EDTA-Free Protease Inhibitors (Roche, Basel, Switzerland) was extracted from H-hI93M/*gad* ([high-expressing] *UCH-L1*$^{I93M/-}$, *Uchl1*$^{gad/gad}$), *gad* and non-Tg mouse midbrains. The extracted samples were loaded as indicated in Fig. 1.

For subfractionation, the cortex and hippocampus were removed from the midbrains of a H-hI93M mouse or a non-Tg littermate and bottom half under the aqueduct were used as the substantia nigra fraction. The fractionation method was modified from that of Kahle et al. (2001). Each sample was homogenized with 9 volumes of 5% SDS/TBS lysis buffer (50 mM Tris–HCl (pH 7.5), 150 mM NaCl, 5% SDS) with Complete EDTA-Free Protease Inhibitors using a 23G syringe. After three times of 10 s sonication, samples were ultra-centrifuged in 130.000 × *g* for 1 h, and the supernatant were pooled as 5% SDS fraction. The pellets were washed with 5% SDS/TBS solution once and further homogenized in 8 M urea/5% SDS/TBS lysis buffer

(8 M urea, 5% SDS, 50 mM Tris–HCl (pH 7.5), 150 mM NaCl) with 23G syringe. The resulting supernatant was used as 8 M urea/5% SDS fraction. The protein concentration was assessed by a DC-protein assay kit (Bio-Rad). 1.25 μg of 5% SDS fraction and 0.5 μg of 8 M urea/5% SDS fraction were subjected to SDS-PAGE using 15% gels (Perfect NT Gel; DRC, Tokyo, Japan). Anti-UCH-L1 (1:5000, RA95101; Ultraclone, Isle of Wight, UK) and anti-β-actin (1:5000, clone AC15; Sigma, St. Louis, MO) were used to detect each protein. Signals were detected using a chemiluminescent SuperSignal West Dura Extended Duration Substrate kit or West Femto Maximum Sensitivity Substrate kit (Pierce, Rochford, IL) and analyzed with a ChemiImager (Alpha Innotech, San Leandro, CA). For the internal control of 8 M urea/5% SDS fraction, 1 μg protein were dot blotted to PVDF membrane and stained with Ponceau S staining (Rane et al., 2004). Statistical analyses were conducted using the two-tailed Student's *t*-test with total of four samples for each group.

For the immunoprecipitation, half of the brain (for hWT/gad) or midbrain region (for L-hI93M/gad) were homogenized in 2 ml ice-cold modified RIPA buffer (50 mM Tris–HCl, pH 7.4; 1% (w/v) Nonidet P40; 0.25% sodium deoxycholate; 150 mM NaCl; 1 mM EDTA) with Complete EDTA-Free Protease Inhibitors and centrifuged at 16,000 × *g* at 4 °C for 20 min. The protein concentration of the resulting supernatants was determined with the Protein Assay Kit (Bio-Rad, Hercules, CA). Immunoprecipitation was performed with a Seize X Mammalian Immunoprecipitation kit (Pierce, Rockford, IL) with some modifications. Briefly, 300 μg of protein was added to a 50 μl slurry of immobilized protein G cross-linked with rabbit polyclonal anti-human UCH-L1 (AB1716; Chemicon, Temecula, CA) or normal rabbit IgG and rotated at 4 °C overnight. The samples were then washed three times with 500 μl of 0.1B buffer (20 mM Tris–HCl, pH 8.0; 0.1 M KCl; 5 mM $MgCl_2$; 10% (w/v) glycerol; 0.1% (w/v) Tween 20; 10 mM β-mercaptoethanol). Elution of samples was performed by adding 20 μl of 5× SDS-PAGE sample buffer, and samples were boiled at 100 °C for 5 min.

2.4. Immunohistochemistry, immunofluorescence and electron microscopy

Brain and peripheral (sciatic) nerve sections from 2-, 7- and 20-week-old mice were analyzed ($n = 3$ for each line) by immunocytochemistry as previously described (Wang et al., 2004; Watanabe et al., 1977) using antibodies to UCH-L1 (1:4000; RA95101, Ultraclone), TH (1:1000; Chemicon) and ubiquitin (1:1000; Sigma–Aldrich, St. Louis, MO). Antibody binding was detected with 3,3′-diaminobenzidine tetrachloride (DAB) or 3-amino-9-ethylcarbazole (AEC) as a peroxidase substrate or Alexa-488- or Alexa-568-conjugated secondary antibodies (Invitrogen, Carlsbad, CA). Sections were then counterstained with hematoxylin. Ultrastructural electron microscopic studies of the substantia nigra were performed as described (Watanabe et al., 1977) using midbrain sections.

2.5. MPTP treatment

For MPTP treatment, the mice received four injections of 30 mg/kg MPTP–HCl intraperitoneally (Research Biochemicals, Natick, MA) in saline at 24-h intervals (Mochizuki et al., 2001).

2.6. Tyrosine hydroxylase-positive cell counting and biochemical analysis

Samples for both histochemistry and biochemical analysis were obtained from the same mouse. Each animal was deeply anesthetized with pentobarbital and perfused transcardially with 10 ml of ice-cold phosphate-buffered saline, and the brain was removed and divided into forebrain and midbrain–hindbrain regions.

For the tyrosine hydroxylase (TH)-positive cell counting, midbrain–hindbrain was fixed with chilled 4% formaldehyde solution (pH 7.4). The procedure of TH-positive cell counting was described previously (Furuya et al., 2004) with minor modifications. Briefly, the substantia nigra was cut into serial sections (30 μm), and every third section was subjected to immunostaining for TH using a polyclonal antibody to TH (a kind gift from I. Nagatsu, Fujita Health University, Aichi, Japan). The Vectorstain Elite ABC kit (Vector Labs, Burlingame, CA) was used for subsequent antibody detection with DAB as a peroxidase substrate. The number of viable TH-positive neurons was assessed by manual counting by a blind observer using coded slides (Furuya et al., 2004). The number of total neuronal cells outside the substantia nigra was counted after Bodian staining in the cerebral cortex (1 mm^2, seven regions per section), cerebellum (total of all lobules) and hippocampus (total number in CA1, CA2, CA3 and dentate gyrus). Statistical analysis were done by one-way ANOVA followed by post hoc test (Fisher's PLSD).

For the biochemical analysis, the striatum was quickly dissected from the forebrain, and the striatal tissue samples were weighed (~30 mg) and homogenized in 10 volumes (w/v) of ice-cold 0.05 M sodium acetate (pH 6.0). Homogenates were centrifuged (18,000 × *g*, 10 min at 4 °C), and the supernatant was frozen immediately on dry ice and stored frozen at −80 °C until use.

For the striatal dopamine measurement, supernatant (50 μl) from the striatal lysate was mixed with an equal volume of 0.2 M perchloric acid containing 0.2 mM EDTA and centrifuged (18,000 × *g*, 10 min at 4 °C), and the supernatant was applied to an HPLC system. Chromatographic separation was achieved using a C18 reversed-phase column (150 mm × 4.6 mm i.d., Model S-100; TOSOH, Tokyo, Japan). The mobile phase (50 mM citrate, 50 mM NaH_2PO_4, 0.1 mM EDTA, 4.36 mM 1-heptanesulfonate, 2.35% acetonitrile, 5.72% MeOH, pH 2.5) was pumped through the chromatographic system at a rate of 1.0 ml/min. A Coulochem electrode array system (ESA Inc., MA) with eight coulometric electrodes was used to quantify the eluted catecholamines and their metabolites. Statistical analysis was done by one-way ANOVA followed by post hoc test (Fisher's PLSD).

TH activity was assayed following the method of Hooper (1997) with minor modifications (Hooper et al., 1997; Naoi et al., 1988). The incubation mixture contained 50 μl of diluted sample and included the following components in a total volume of 200 μl: 0.2 M sodium acetate (pH 6.0), 0.2 M glycerol, 20,000 U/ml catalase, 1.0 mM 6-MPH4, 4.0 U/ml dihydropteridine reductase, 1 mM NADPH and 200 μM L-tyrosine. Incubations were carried out at 37 °C for 10 min in a shaking water bath. Reactions were terminated by adding 600 μl of ice-cold 0.33 M perchloric acid, 17 mM EDTA including 50 pmol of α-methyl DOPA as the internal standard. The L-DOPA produced was extracted onto alumina, and the catechols were eluted with 0.16 M acetic acid followed by 0.02 M phosphoric acid. A sample incubated on ice instead of 37 °C was used as a blank. The amount of L-DOPA was quantified with the HPLC system, as mentioned above. Statistical analysis was done by one-way ANOVA.

2.7. Silver staining

Sixty-micrometer brain sections from 12-week-old mice ($n = 3$ for each group) were stained using FD NeuroSilver kit (FD Neuro-Technologies, Catonsville, MD) according to the manufacturer's protocol to detect argyrophilic grain-positive degenerating neurons.

2.8. Behavioral tests

H-hI93M mice and non-Tg littermates were used for all behavioral analyses. For the accelerated rota-rod test, 20–25-week-old mice were placed on the rod (Ohara, Japan) at a speed of 5 rpm, and the speed was accelerated to 50 rpm in 5 min. The length of time that each mouse was able to remain on the rod before falling was recorded. For the locomotor activity test, 11–13-week-old or 20–23-week-old mice were placed separately in a home cage 4 days before the beginning of analysis for habituation. Two to four mice were monitored at once for locomotor activity on the home cage monitor (Ohara, Japan) for 63 h beginning from 5:30 p.m. All mice were housed with a 12 h light/dark cycle, with the light cycle beginning at 8 a.m. The last 12 h of active night were used for the analysis. Mice were weighed after the analysis; there were no differences between the weights H-hI93M and non-Tg mice (data not shown). Statistical analyses were conducted using the two-tailed Student's *t*-test.

3. Results

3.1. Generation of transgenic mice expressing human *UCHL1*^{I93M} in neurons of the substantia nigra

The human *PDGF-B* promoter was used to drive expression of the human *UCHL1* in Tg mice (Fig. 1A) (Sasahara et al., 1991). Germline transmission of *hUCHL1*^{I93M} was obtained in two independent Tg mouse lines (denoted L-hI93M and H-hI93M, where L and H denote low and high expression, respectively). Germline transmission of *hUCHL1*^{WT} was obtained in one Tg mouse line (denoted hWT). The levels of transgenic mRNA and endogenous *Uchl1* mRNA were assessed by quantitative RT-PCR using primers designed to amplify specifically the *UCHL1* transgene and mouse *Uchl1*, respectively. The estimated relative expression of *UCHL1* among the transgenic lines was H-hI93M > hWT > L-hI93M. The ratio of endogenous mouse *Uchl1* transcripts to transgenic human *UCHL1* transcripts was 111 in H-hI93M, 739 in hWT and 6015 in L-hI93M ($n = 3$ for each line).

At the amino acid level, human and mouse UCH-L1 differ at only 11 discrete positions, and endogenous UCH-L1 is one of the most abundant protein in the brain. Therefore, we were not able to make distinction between the exogenous human UCH-L1 and endogenous mouse UCH-L1 in the brains of Tg mice (data not shown) using immunoblotting analysis with several antibodies against human UCH-L1 from different companies (Chemicon; UltraClone; Medac; Biogenesis). To ascertain the expression of transgene product, we used *gad* mice, which lack endogenous UCH-L1 (Saigoh et al., 1999). We mated mice

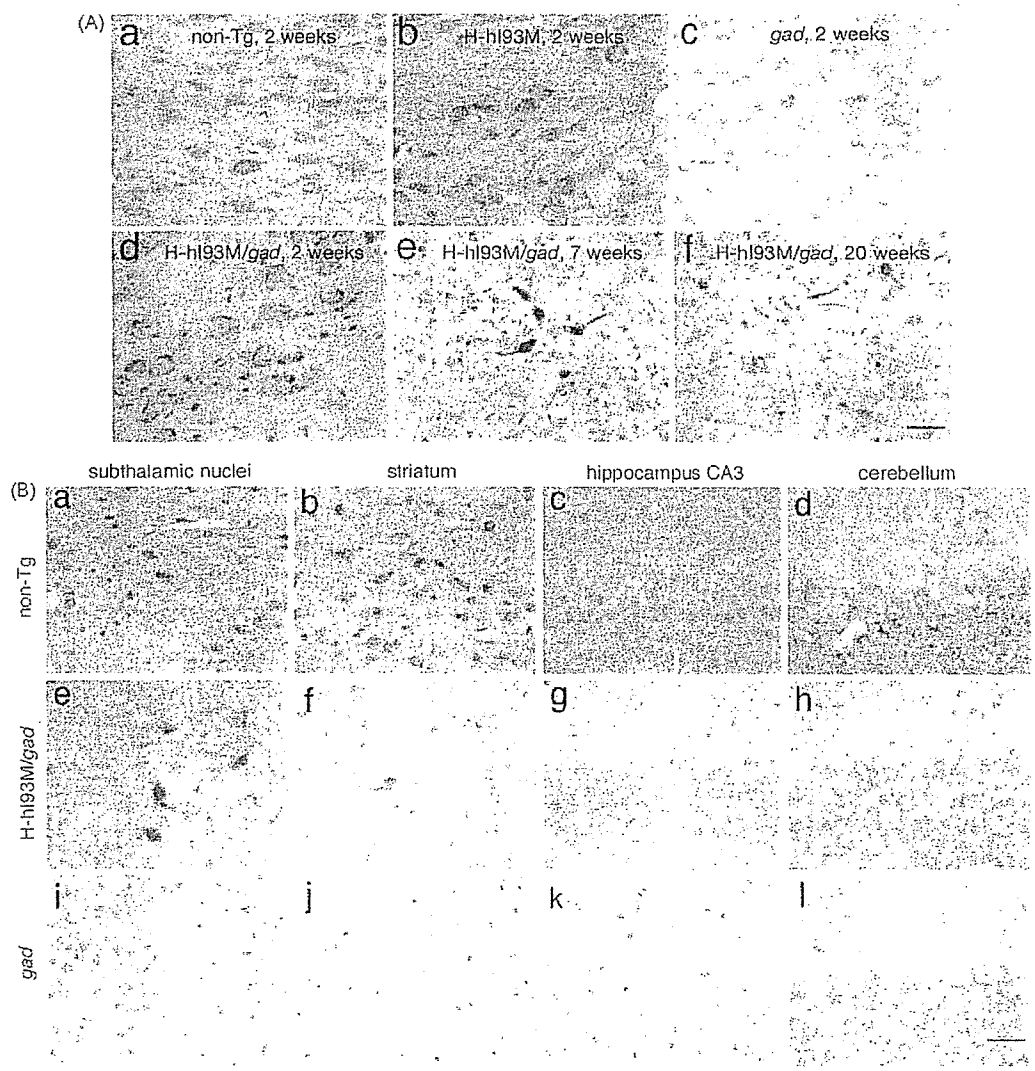

Fig. 2. Immunohistochemistry of UCH-L1 in coronal sections of the substantia nigra (A) and regions outside the substantia nigra (B) in H-hI93M, H-hI93M/*gad* and non-Tg mice. (A) Non-Tg mice (a). H-hI93M mice on a C57BL/6J background (b) and *gad* mice (c) at 2 weeks of age and H-hI93M/*gad* mice at 2 weeks (d), 7 weeks (e) and 20 weeks (f) of age. Neurons expressing UCH-L1 in the substantia nigra decreased in number and area, and densely stained neurons were observed in the aged substantia nigra. Scale bar: 30 μm. (B) UCH-L1 immunohistochemistry of coronal sections at the level of the subthalamic nuclei (a, e, i), striatum (b, f, j), hippocampus CA3 (c, g, k) and cerebellum (d, h, l). Upper row (a–d), non-Tg mice; middle row (e–h), H-hI93M/*gad* mice; lower row (i–l), *gad* mice. All mice were examined at 2 weeks of age. Scale bar: 30 μm.

from each transgenic line with mice homozygous for the *Uchl1*$^{gad/gad}$ allele (*gad* mice). Detergent-soluble (1% Triton X-100) fractions of mouse midbrain from H-hI93M/*gad* (*UCHL1*$^{I93M/-}$, *Uchl1*$^{gad/gad}$) at 2 and 15 weeks of age were subjected to SDS-PAGE and immunoblotted with anti-UCH-L1. We detected human UCH-L1 expression in H-hI93M/*gad* brains (Fig. 1B). Compared with endogenous mouse UCH-L1, which constitutes 1–2% of neuronal proteins, human UCH-L1 expression was substantially lower in H-hI93M/*gad* brains (~1% of endogenous UCH-L1 at 2 weeks of age; Fig. 1B). Interestingly, the level of transgenic human UCH-L1 was lower at 15 weeks than at 2 weeks of age (Fig. 1B). Although we could not detect human UCH-L1 in L-hI93M/*gad* and hWT/*gad* by standard immunoblotting methods, we were successful in detecting it by immunoprecipitation (Fig. 1C). These data suggest the expression of the human UCH-L1 in L-hI93M and hWT mice, which were much lower than in H-hI93M mice.

UCH-L1 is a cytosolic protein predominantly expressed in neuronal cells including dopaminergic neurons at substantia nigra with diffuse localization (data not shown). Thus, we next examined the immunohistochemical localization of the transgene products. In agreement with the data obtained by Western blotting analysis, UCH-L1-immunoreactive cells were not observed in any brain region, including the substantia nigra, of the L-hI93M/*gad* and hWT/*gad* mice (data not shown). In H-hI93M/*gad* mice, however, human UCH-L1^{I93M} was detected in the substantia nigra, the region that contains the central pathological lesions in PD, with relatively high intensities (Fig. 2A). Subthalamic nuclei, striatum, hippocampus CA3 and cerebellum also contained UCH-L1 immunoreactive cells in H-hI93M/*gad* mice (Fig. 2B). As with the previous report that CAT expression under control of the *PDGF-B* promoter in transgenic mice localizes to neuronal cell bodies (Sasahara et al., 1991), most UCH-L1-immunoreactive cells in H-hI93M/*gad* mice had a neuronal morphology (Fig. 2). Western blotting analysis of midbrain lysates showed a reduction of transgenic UCH-L1^{I93M} at 15 weeks of age as compared with that at 2 weeks in H-hI93M/*gad* mice (Fig. 1B). Thus, we also performed immunohistochemical analysis of UCH-L1 on substantia nigra from 2-, 7- and 20-week-old H-hI93M/*gad* mice. We found many UCH-L1-positive neurons at 2 weeks. The number of positive cells had decreased by 7 weeks, however, at which time small-sized and densely stained neurons were observed, and UCH-L1-positive cells were barely

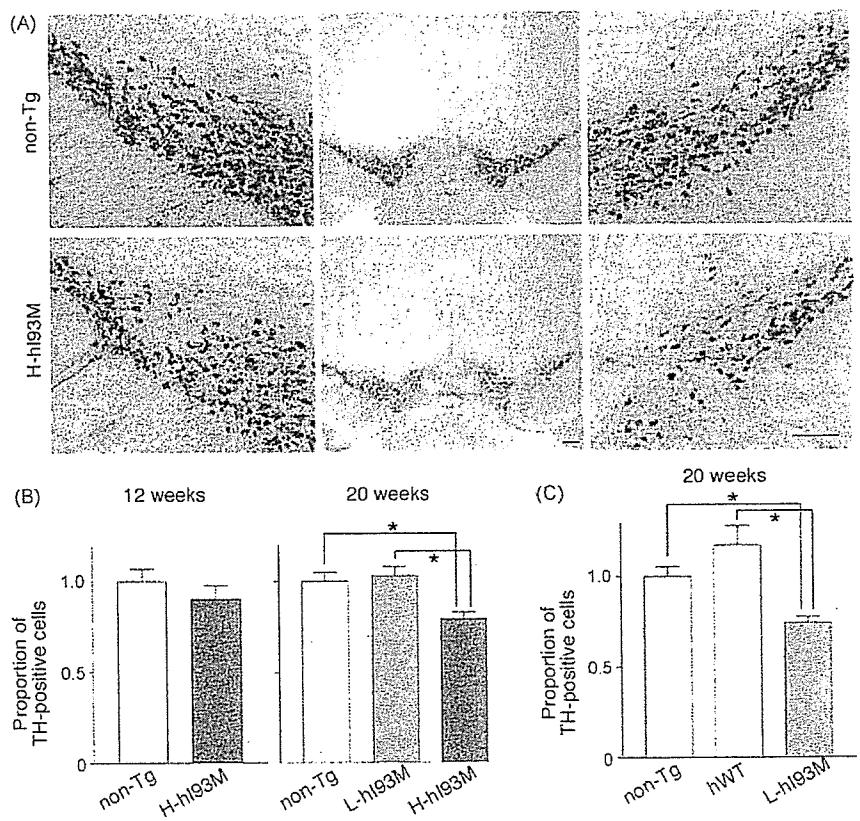

Fig. 3. TH-positive neurons of hI93M Tg mice were reduced as the animals aged. (A) Immunohistochemical staining of the substantia nigra with anti-TH in non-Tg (upper panels) and H-hI93M (lower panels) mice at 20 weeks of age. Scale bar: 1 mm. Left and right panels in the figure correspond to the left and right part of the middle panel, respectively. (B) Proportion of neurons stained with anti-TH in the substantia nigra from non-Tg and hI93M mice at 12 weeks (left panel) and 20 weeks (right panel) of age. Cell numbers were normalized to those for the non-Tg mice. Values are the mean ± S.E.M.; $n = 10$ Significance was examined by a one-way ANOVA. $^{*}p < 0.01$. (C) The number of TH-positive cells in the substantia nigra from 20-week-old non-Tg ($n = 5$), hWT ($n = 3$) and L-hI93M mice ($n = 5$) after treatment with MPTP. The cell numbers were normalized to those for non-Tg mice. Values are the mean ± S.E.M. Significance was examined by a one-way ANOVA. $^{*}p < 0.001$.